Fluid Dynamics &
Materials Processing

Tech Science Press

http://doi.org/10.32604/fdmp.2026.082984

ARTICLE

Thermo-Hydraulic Performance and Entropy Generation Analysis of Serpentine and Straight Tubes with Twisted Tape Inserts Using SST k-ω Turbulence Modeling

Conghai Chen[1], Dingran Sun[2], Yikai Chen[2], Jianxin Xu[2,*] and Hua Wang[2]

[1]State Key Laboratory of Complex Nonferrous Metal Resources Clean Utilization, School of Metallurgical and Energy Engineering, Kunming University of Science and Technology, Kunming, China
[2]Faculty of Metallurgical and Energy Engineering, Kunming University of Science and Technology, Kunming, China
*Corresponding Author: Jianxin Xu. Email: xujianxina@163.com

Received: 26 March 2026; Accepted: 12 May 2026; Published: 30 June 2026

ABSTRACT: Serpentine heat exchangers are extensively used in energy and chemical engineering owing to their compact geometry and high thermal performance. To improve their efficiency, three-dimensional numerical simulations are conducted using the SST k-ω turbulence model for both serpentine and straight tubes fitted with twisted tape inserts. Three twist ratios (y = 5.77, 8.57, 12.48) are examined across a Reynolds number range of 10,000 to 22,000. Results show that the average Nusselt number increases with Reynolds number, while the friction factor decreases. In particular, due to curvature-driven secondary motions, serpentine configurations consistently outperform straight tubes in thermal performance. The addition of twisted tapes intensifies fluid mixing through strong swirl generation, disrupting the thermal boundary layer and significantly enhancing heat transfer, albeit with increased flow resistance. Among all cases, the lowest twist ratio (y = 5.77) generates the strongest swirl intensity and highest turbulent kinetic energy, yielding maximum thermal augmentation but also the greatest pressure drop. Performance Evaluation Criterion analysis indicates $PEC > 1$ for all twisted tape configurations under equal pumping power, confirming an overall beneficial trade-off between enhancement and hydraulic penalty. Entropy generation results further demonstrate that improved thermal performance is accompanied by higher irreversibility. Overall, the combination of serpentine geometry with low to moderate twist ratios offers the most favorable thermo-hydraulic balance for compact heat exchanger optimization.

KEYWORDS: Serpentine tube; twisted tape inserts; turbulent heat transfer enhancement; entropy generation analysis; thermo-hydraulic performance

1 Introduction

Serpentine tube heat exchangers are widely employed in various industrial applications, including energy chemistry, power engineering, and renewable energy utilization, owing to their compact structure, strong adaptability, and high heat transfer efficiency [1–3]. In recent years, increasing demands for energy efficiency and conservation have stimulated extensive research on serpentine tubes and heat transfer enhancement techniques. To improve the heat transfer performance of heat exchanger tubes, various flow-disrupting elements have been proposed, particularly through the insertion of different types of inserts to intensify fluid mixing. Dong et al. [4] developed numerical models of triangular, rectangular, and sector-shaped internally ribbed tubes to enhance heat dissipation capacity. Their analysis demonstrated

that, compared with smooth circular tubes, internally ribbed tubes significantly improve heat transfer performance by disturbing the boundary layer and promoting fluid mixing, albeit with an associated increase in pressure drop. Wei et al. [5] investigated the effects of turbulator geometry, row number, and inlet/outlet configurations on the thermal and hydraulic performance of an AlN-based microchannel heat sink using thermo-fluid-structure coupled simulations. The results revealed that circular baffles are most effective in suppressing vortex stagnation, leading to a substantial increase in the local Nusselt number and overall heat transfer efficiency. Ahirwar et al. [6] experimentally evaluated the thermohydraulic performance of double-pipe heat exchangers (DPHEs) equipped with novel coil inserts. Five different coil pitch ratios were examined, and the results indicated that the thermal performance factor (TPF) of all configurations exceeded unity, confirming the effectiveness of coil inserts for heat transfer enhancement. Singh et al. [7] examined the influence of single-type and multi-V-cut twisted-tape inserts on the Nusselt number (Nu), friction factor (f), and performance evaluation criterion (PEC) in double-pipe heat exchangers. The findings suggested that V-cut twisted tapes offer superior performance at relatively low Reynolds numbers within the turbulent regime, where heat transfer enhancement is more pronounced. Marzouk et al. [8] explored the combined effects of twisted-tape inserts (TTIs) and tungsten carbide/water nanofluids on the thermal performance and compactness of twin-tube spiral heat exchangers. The results demonstrated that the synergistic interaction between TTIs and nanofluids enhances turbulence intensity, leading to higher Nusselt numbers and improved overall thermal performance. Sahin et al. [9] investigated the effect of a novel hemispherical turbulator configuration on the melting process of RT35 phase-change material (PCM) within a double-pipe heat exchanger. The study revealed the potential to further enhance heat exchanger efficiency by optimizing the design of the turbulence-promoting elements and strategically integrating the phase-change material.

The structural design and performance optimization of serpentine tube heat exchangers have evolved along multiple innovative directions. Shahsavar et al. [10] compared serpentine tubes with circular, triangular, and rectangular cross-sections in photovoltaic/thermal (PV/T) systems, reporting that rectangular tubes achieve superior electrical and overall energy efficiencies. Reddy et al. [11] proposed a curved serpentine (CS-θ) chaotic coil configuration, which exhibits enhanced thermohydraulic performance compared with conventional serpentine and spiral coils; subsequently, Awasthi et al. [12] optimized the coil switching angle and demonstrated that the modified structure significantly improves thermohydraulic performance under laminar flow conditions. Sun et al. [13] introduced a branched serpentine channel design to enhance temperature uniformity and reduce pressure drop in electric vehicle battery thermal management systems. Singh et al. [14] designed serpentine cooling channels arranged along the blade chord, achieving a heat transfer coefficient approximately twice that of smooth tubes under rotating conditions. Tanthadiloke et al. [15] developed a W-shaped serpentine heat exchanger, which improved heat dissipation performance by approximately 23% compared with conventional U-shaped configurations, highlighting the critical role of structural innovation in performance enhancement. Moreover, due to the combined effects of curvature-induced secondary flow, buoyancy forces, and flow instabilities, serpentine tubes generally exhibit superior convective heat transfer performance compared with straight tubes. Fathalla et al. [16] reported that the mass transfer coefficient of serpentine tubes can reach 4.12–5.36 times that of straight tubes, while Zhang et al. [17] showed that buoyancy effects in supercritical CO_2 flows can enhance heat transfer performance by up to 23%. Han et al. [18] and Wang et al. [19] investigated the convective heat transfer characteristics of supercritical LNG in horizontal serpentine tubes, revealing that the heat transfer coefficient peaks as the fluid temperature approaches the pseudo-critical temperature. They also noted that increasing the mass flow rate mitigates heat transfer deterioration, whereas higher outer wall temperatures

weaken heat transfer performance. In addition, the curved sections of serpentine tubes further enhance heat transfer through intensified secondary flow.

A wide range of techniques has been proposed to enhance heat transfer performance [20–22]. Increasing the effective heat transfer area is one of the most common approaches, typically achieved through the use of non-circular tubes—such as finned, corrugated, and spiral tubes—or by incorporating surface structures including fins and protrusions. Mechanical agitation and vibration can disrupt the boundary layer and intensify turbulence, thereby improving the heat transfer coefficient. The insertion of flow-disturbing elements, such as twisted tapes or helical coils, modifies flow patterns and promotes heat transfer enhancement. In addition, the use of additives, including nanoparticles [23] and surfactants, can alter thermophysical properties such as thermal conductivity and viscosity, leading to improved heat transfer performance. Phase-change heat transfer processes, including evaporation and condensation [24], utilize latent heat to achieve high heat transfer efficiency. Surface modification techniques, such as coating or roughening, further enhance heat transfer by increasing surface roughness and effective area. Microchannel technology [25] reduces characteristic flow dimensions, thereby increasing fluid velocity and turbulence intensity [26], which contributes to improved heat transfer efficiency. With the advancement of numerical methods, significant progress has also been made in studies of enhanced heat transfer based on finite element analysis and mixed nanofluids. For instance, Mebarek-Oudina et al. [27] employed the Galerkin finite element method to investigate turbulent heat transfer of ternary hybrid nanofluids in shell-and-tube heat exchangers, demonstrating that increasing particle volume fraction and flow velocity markedly enhances heat transfer performance. Fayz-Al-Asad et al. [28] analyzed mixed convection in magnetofluids within a wavy enclosure, showing that geometric configurations and dimensionless parameters significantly influence heat transfer characteristics. Furthermore, Kanti et al. [29,30] examined the thermal performance of Al_2O_3–TiO_2 and other hybrid nanofluids under turbulent conditions through both experimental and numerical approaches. Their findings indicated that hybrid nanofluids not only enhance the heat transfer coefficient but also reduce entropy generation and improve overall thermodynamic performance. These studies suggest that the integration of advanced numerical methods with novel working fluids represents a key direction in contemporary heat transfer enhancement research.

Internal twisted-tape inserts have attracted considerable research interest due to their simple fabrication, low cost, and ease of retrofitting into existing equipment. Liaw et al. [31] numerically investigated the turbulent heat transfer characteristics of helical tubes equipped with internal twisted tapes under constant wall temperature conditions, demonstrating that the introduction of twisted tapes enhances radial secondary flow intensity and significantly improves heat transfer performance. Kurnia et al. [32] conducted a numerical study on the flow behavior and associated heat transfer in helical tubes, revealing that, compared with conventional straight-tube heat exchangers, the incorporation of twisted tapes can enhance heat transfer performance by up to fourfold. Bozzoli et al. [33] reported that twisted-tape inserts outperform smooth tubes in terms of heat transfer under both laminar and turbulent flow regimes; meanwhile, Chourasia et al. [34] numerically examined the effects of trapezoidal-cut twisted tapes inserted into circular pipes on fluid flow and heat transfer characteristics, showing that, particularly under turbulent conditions, trapezoidal-cut configurations—especially double-cut designs—can markedly enhance heat transfer, making them an effective passive enhancement technique. Marzouk et al. [35] further investigated the combined effects of perforated twisted tapes and alumina nanofluids in a double-pipe heat exchanger, demonstrating that their synergistic interaction significantly increases the Nusselt number and flow efficiency under turbulent conditions, with enhancement becoming more pronounced at higher nanoparticle volume fractions. Azmi et al. [36] explored the interaction between nanofluids and twisted tapes, indicating

that a lower twist ratio can substantially improve the heat transfer coefficient. In addition, extensive studies have systematically examined the influence of geometric parameters of twisted tapes—including twist ratio, perforation structure, and tapered configurations—on thermohydraulic performance, and have suggested that composite enhancement strategies, such as the combination of multi-strand twisted tapes with helical corrugated tubes, can further improve heat transfer performance [37–40].

Although previous studies have separately examined the effects of serpentine tube structures and twisted-rib inserts on flow and heat transfer performance, most existing research has focused on individual enhancement techniques, resulting in a lack of systematic understanding of flow structure evolution and heat transfer mechanisms under their combined effects. In particular, the interaction mechanisms between curvature-induced secondary flows and twisted-tape-induced vortices, the modulation of turbulent structures, and the intrinsic trade-off between energy dissipation and heat transport during heat transfer enhancement remain insufficiently explored. To address these gaps, this study establishes a three-dimensional turbulent numerical model to systematically investigate the influence of twisted inserts on the flow and heat transfer characteristics in serpentine tubes. Special attention is given to the synergistic enhancement effects arising from the interaction between twisted inserts and curved geometries under varying twist ratios (y = 5.77, 8.57, 12.48) and Reynolds numbers (10,000 $\leq Re \leq$ 22,000). The underlying mechanisms are elucidated through detailed analyses of flow structures, turbulence characteristics, and temperature field distributions, with particular emphasis on the coupling between curvature-induced secondary flows and twisted-tape vortices. Furthermore, entropy generation analysis is combined with performance evaluation criteria to quantify the trade-off between heat transfer enhancement and flow resistance from both thermodynamic and engineering perspectives. Finally, empirical correlations for heat transfer and friction characteristics are developed, providing theoretical support and predictive tools for the optimal design of enhanced serpentine tube heat exchangers.

2 Model Composition and Introduction

Based on the conservation of energy principle, two single-phase flow models were established in this study: a straight pipe model with a twisted-tape insert and a serpentine pipe model. The working fluid is water at an inlet temperature of 333.15 K. The twisted tape, a simple and easy-to-install passive vortex generator, is typically fabricated from a thin metallic strip (e.g., stainless steel or aluminum) with a thickness of approximately 1 mm through a twisting process, forming a helical structure that is either closely fitted to the inner wall of the pipe or mounted along the pipe centerline. The degree of twisting is commonly characterized by the twist ratio, y, defined as the ratio of the axial length H required for a 180° rotation of the tape to its characteristic width (or pipe inner diameter) b, i.e.,

$$y = \frac{H}{b} \tag{1}$$

The specific geometry and dimensions of the model are shown in Figs. 1 and 2, and the detailed structural parameters are listed in Table 1.

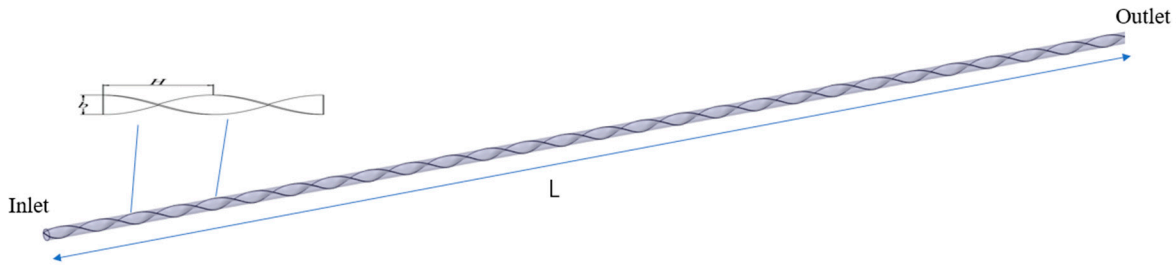

Figure 1: Schematic diagram of a straight tube with a twisted tape and the twisted tape itself.

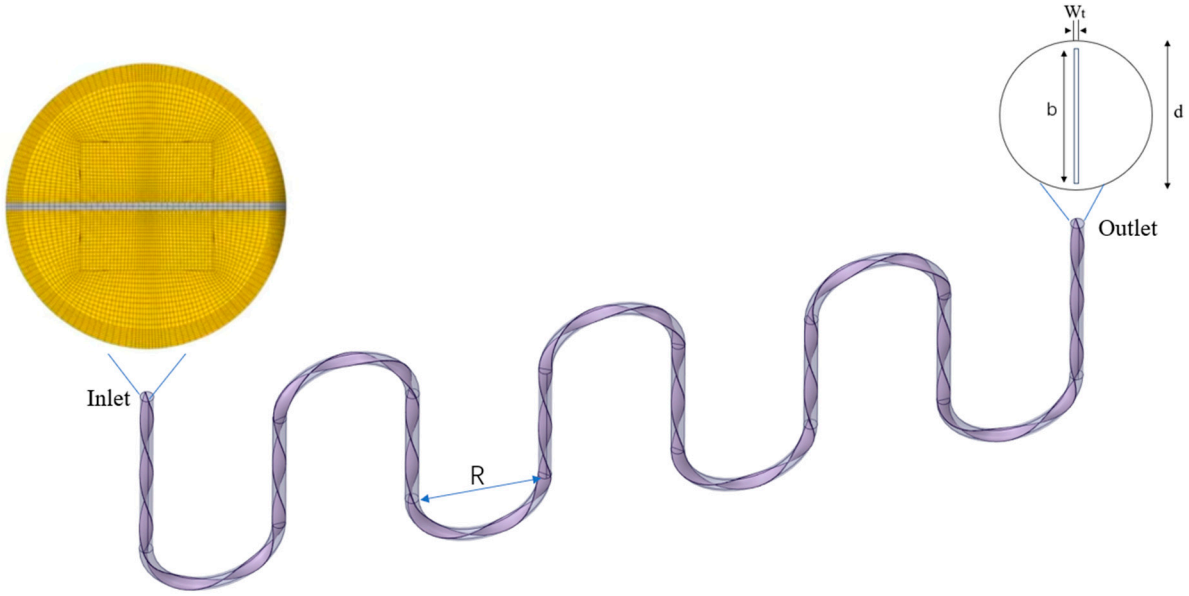

Figure 2: Schematic diagram of the serpentine tube with twisted tapes and grid division.

Table 1: Model Parameters.

Parameter	Numerical Values	Unit
L	1.6792	m
d	8×10^{-3}	m
R	4×10^{-2}	m
Tin	333.15	K
$Twall$	293.15	K
b	7.8×10^{-3}	m
Wt	2×10^{-4}	m
H	4.5×10^{-2}	m
y	5.77	-

2.1 Governing Equations

To describe the incompressible turbulent flow and heat transfer processes within a serpentine tube, this paper establishes a system of governing equations based on the Reynolds-averaged Navier–Stokes (RANS) equations. This system of equations is derived by time-averaging the instantaneous Navier–Stokes equations and enclosing the Reynolds stress term using a turbulence model. Considering the changes in

energy and momentum in the turbulent flow of water within the tube, the conservation equations for this flow are given by the following equations:

Continuity equation:

$$\nabla \cdot u = 0 \tag{2}$$

Momentum equation:

$$\frac{\partial u}{\partial t} + (u \cdot \nabla)u = -\frac{1}{\rho}\nabla p + \nu \nabla^2 u - \nabla \cdot \overline{u'u'} \tag{3}$$

Energy equation:

$$\frac{\partial \left(\rho c_p T\right)}{\partial t} + \nabla \cdot \left(\rho c_p u T\right) = \nabla \cdot (\lambda \nabla T) \tag{4}$$

In the above equation, ρ represents density, u represents velocity vector, μ represents viscosity coefficient, p represents pressure, c_p is specific heat capacity. u' represents the velocity fluctuation, and the Reynolds stress term $-u'u'$ is typically expressed using the Boussinesq hypothesis as a function of the turbulent viscosity and the gradient of the time-averaged velocity. The turbulent viscosity is not a constant but a flow-dependent property, and its determination requires a suitable turbulence model. In the present study, the SST k-ω model is employed for this purpose, as described in Section 2.2.

2.2 Turbulence Model

The appropriate selection of a turbulence model is essential for accurately simulating turbulent flow. Due to the inherent nonlinearity, wide range of spatial and temporal scales, and transient characteristics of turbulence, direct numerical simulation (DNS) of the instantaneous Navier–Stokes equations remains computationally prohibitive for most engineering applications. Consequently, turbulence models are employed to achieve closure of the Reynolds stress terms. In the present study, the shear stress transport SST k-ω model is adopted. Originally proposed by Menter, this model combines the advantages of the k-ω formulation in the near-wall region and the k-ε formulation in the free stream through a blending function. The transport equations for the turbulent kinetic energy (k) and the specific dissipation rate (ω) are given as follows:

Turbulent kinetic energy (κ) equation:

$$\frac{\partial(\rho k)}{\partial t} + \frac{\partial(\rho u_i k)}{\partial x_i} = P_k - \beta^* \rho k \omega + \frac{\partial}{\partial x_j}\left[(\mu + \sigma_k \mu_t)\frac{\partial k}{\partial x_j}\right] \tag{5}$$

Equation for specific dissipation rate (ω):

$$\frac{\partial(\rho \omega)}{\partial t} + \frac{\partial(\rho u_i \omega)}{\partial x_i} = \alpha \rho S^2 - \beta \rho \omega^2 + \frac{\partial}{\partial x_j}\left[(\mu + \sigma_\omega \mu_t)\frac{\partial \omega}{\partial x_j}\right] + 2(1 - F_1)\rho \sigma_\omega^2 \frac{1}{\omega}\frac{\partial k}{\partial x_j}\frac{\partial \omega}{\partial x_j} \tag{6}$$

where P_k represents the turbulent kinetic energy generation term caused by the average velocity gradient. The core idea of this model is to describe the vortex dynamics of turbulence more accurately through

improved transport equations. Specifically, the model controls the region switching by introducing a mixing function F_1:

$$F_1 = \tanh^4\left\{\min\left[\max\left(\frac{\sqrt{k}}{\beta^* wy}, \frac{500\nu}{y^2\omega}\right), \frac{4\rho\sigma w^2 k}{CD_{kw}y^2}\right]\right\} \tag{7}$$

When F_1 = 1, the model behaves as a k-ω mode in the near-wall region to better capture turbulent behavior within the boundary layer; while in the region far from the wall (F_1 = 0), the model switches to a k-ε mode, thus effectively solving the problem that the traditional k-ω model is too sensitive to free-flow boundary conditions. To more accurately predict flow separation, the SST k-ω model considers the transmission of turbulent shear stress when defining the turbulent viscosity μ_t:

$$\mu_t = \frac{a_1 pk}{\max(a_1\omega, SF_2)} \tag{8}$$

where S is the invariant of the strain rate tensor, and F_2 is the second mixing function. Through this adaptive turbulence length scale constraint, the model can provide relatively accurate results in complex flows, especially in the transition and separated flow regions, exhibiting strong resistance to discretization errors and high numerical stability. The standard constants of the SST k-ω turbulence model (Menter, 1994) are adopted in the present simulations, as listed in Table 2.

Table 2: Table of Constant Values in Turbulence Model Equations.

Constant	Value	Constant	Value
β^*	0.09	αk	0.85
$\sigma_{\omega 1}$	0.5	α_1	0.5556
β_1	0.075	σ_{k2}	1.0
$\sigma_{\omega 2}$	0.856	α_2	0.44
β_2	0.0828	a_1	0.31

Note: These constants are implemented in ANSYS Fluent as default values for the SST k-ω model.

2.3 Basic Assumptions

Fluid flow and heat transfer within a pipe constitute a complex three-dimensional physical process. To improve computational efficiency while ensuring accuracy and to highlight the primary physical mechanisms, this study makes the following reasonable assumptions regarding fluid flow and heat transfer within the computational domain:

(1) The fluid is an incompressible Newtonian fluid, and its physical properties remain constant throughout the calculation;
(2) The flow is steady-state; the effects of time variation on flow and heat transfer are not considered;
(3) Thermal radiation effects within the fluid are neglected; only convection and conduction are considered;
(4) The effects of gravity and natural convection are neglected; only forced convective heat transfer is considered;
(5) The wall surface satisfies a no-slip boundary condition, meaning the fluid velocity at the wall is zero;
(6) The effects of other minor energy loss terms are not considered.

While ensuring computational accuracy, the above assumptions effectively reduce model complexity, facilitating the analysis of flow and heat transfer mechanisms.

2.4 Boundary Conditions

To investigate the flow and heat transfer characteristics within a serpentine tube at different Reynolds numbers, the following boundary conditions were used in the numerical simulation:

Inlet: A constant velocity boundary condition is applied at the inlet. By varying the flow velocity to control the Reynolds number, the flow behavior under different flow intensities is simulated. The Reynolds number is defined as follows:

$$Re = \frac{\rho U_{in} D}{\mu} \tag{9}$$

where ρ is the fluid density, U_{in} is the inlet average velocity, D is the pipe diameter, and μ is the viscosity coefficient. In this study, seven different Reynolds numbers were set: 10,000, 12,000, 14,000, 16,000, 18,000, 20,000, and 22,000, corresponding to different inlet velocities U_{in}. This ensures the flow is in a turbulent state, allowing for the analysis of flow and heat transfer characteristics at high Reynolds numbers.

Outlet: The outlet was set as a constant pressure outlet, applying zero gauge pressure (i.e., relative pressure of 0), and assuming the temperature gradient of the fluid in the outlet direction is zero, i.e.,

$$p|_{\text{outlet}} = 0, \quad \left.\frac{\partial T}{\partial x}\right|_{\text{outlet}} = 0 \tag{10}$$

This setting implies that the fluid is smoothly discharged from the system and assumes that there is no significant temperature change at the outlet, which helps to maintain numerical stability. The pipe wall is set to a constant wall temperature condition, i.e., the wall temperature is a fixed value *Tw*, and no-slip boundary conditions are applied to the velocity components. This boundary condition is used to study the influence of the wall on the temperature and velocity fields of the fluid in forced convection heat transfer problems.

3 Numerical Methods

The computational domain was established to solve the governing equations of momentum and energy conservation, with the prescribed boundary conditions implemented in ANSYS Fluent. The computational mesh was generated and defined using ANSYS Meshing. A pressure-based solver was employed, and the governing equations were discretized using a second-order upwind scheme to ensure numerical accuracy. In addition, pressure–velocity coupling was achieved using the semi-implicit method for pressure-linked equations (SIMPLE) algorithm. The convergence criterion for all residuals was set to 10^{-6}. To ensure grid-independent results, a mesh independence study was performed by systematically increasing the number of mesh elements. Straight-tube and serpentine-tube configurations were evaluated under identical operating conditions until further mesh refinement produced no significant changes in the numerical results. The final mesh sizes for the straight tube and serpentine tube were approximately 2.0 million and 3.5 million elements, respectively. These mesh densities were selected because they satisfied the accuracy requirements while maintaining reasonable computational cost. As shown in Fig. 3 (mesh independence verification), when the number of mesh elements increased from 3.0 million to 3.5 million, the relative change in pressure drop was approximately 1.1%, while the change in the average Nusselt number was approximately 1.2%. These results indicate that the numerical predictions are insensitive to further mesh refinement and therefore satisfy the mesh independence criterion. To ensure that the prescribed residual convergence criterion was fully achieved, the maximum number of iterations was set to 5000.

To further improve the reliability of the numerical results, the performance of several turbulence models was also evaluated. The predictive capabilities of four turbulence models—Standard k-ε, RNG k-ε, Standard k-ω, and SST k-ω—were compared and validated against classical empirical correlations. As shown in Fig. 4, the SST k-ω model provided the most accurate prediction of the Nusselt number, exhibiting the closest agreement with the empirical correlation. For the friction factor, the Standard k-ω and SST k-ω models produced similar results, and both showed stable predictive performance.

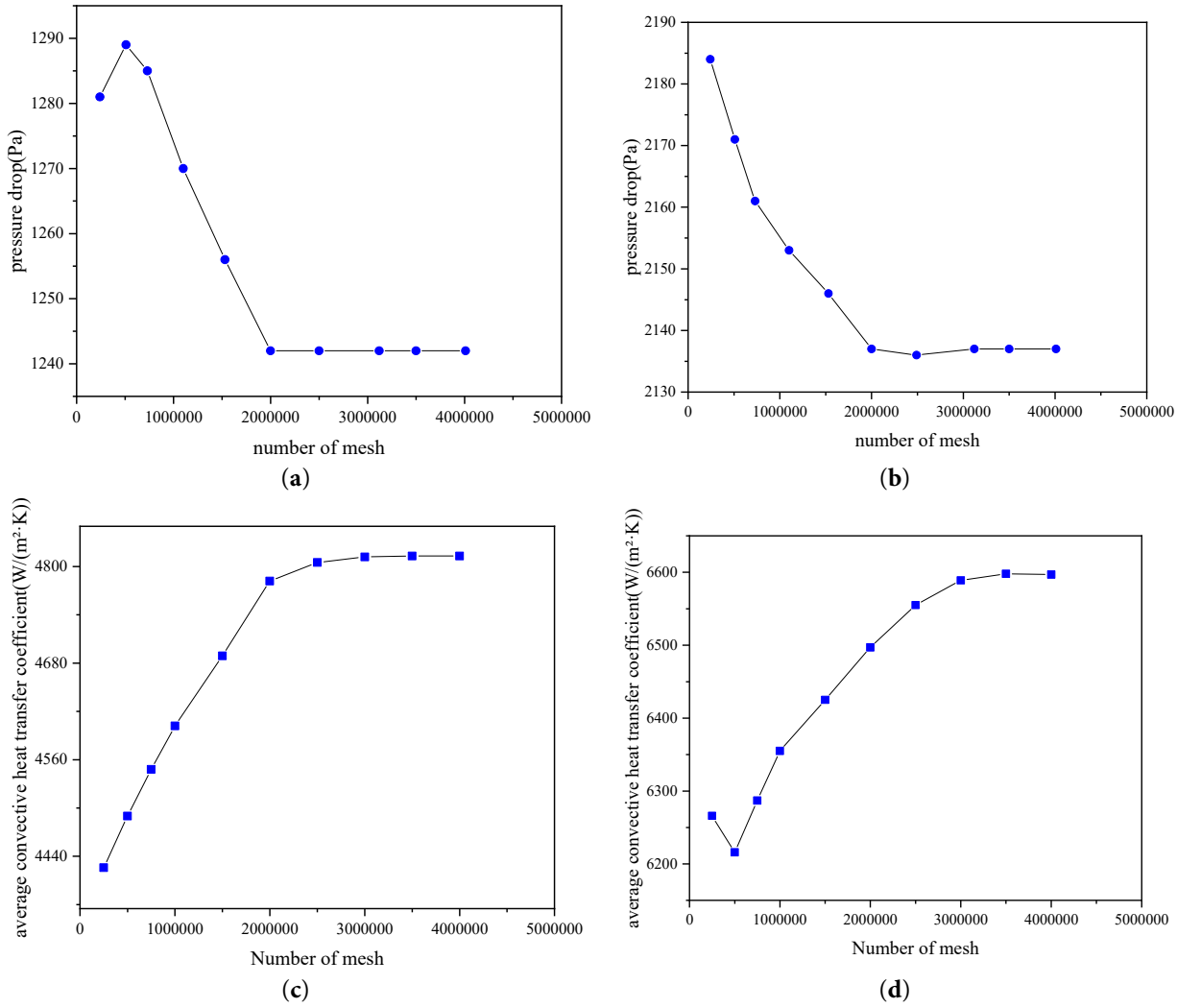

Figure 3: Mesh independence verification. (**a**) shows the relationship between pressure drop and mesh number for the serpentine tube without twisted tape. (**b**) shows the relationship between pressure drop and mesh number for the straight tube without twisted tape. (**c**) shows the relationship between average convective heat transfer coefficient and mesh number for the straight tube without twisted tape. (**d**) shows the relationship between average convective heat transfer coefficient and mesh number for the serpentine tube without twisted tape.

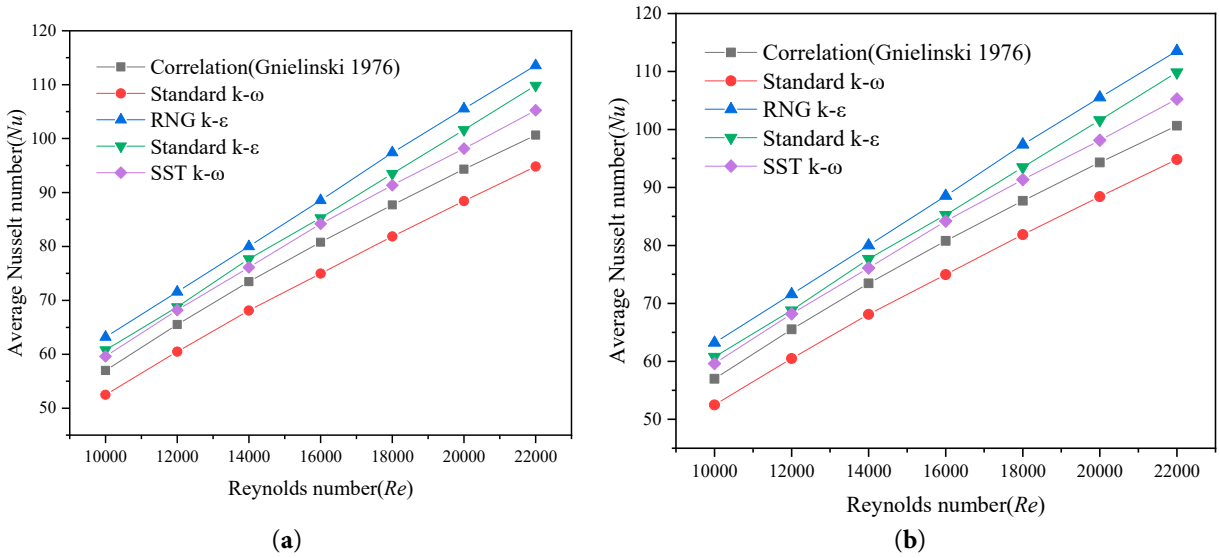

Figure 4: Comparison of results from various turbulence models and empirical formulas for straight pipes without twisting tape at a wall temperature of 293.15 K. (**a**) shows the friction coefficient, and (**b**) shows the average Nusselt number.

4 Results and Discussion

4.1 Model Validation

To ensure the scientific soundness and reliability of the numerical results, the computational model must be rigorously validated. Model validation is a crucial step in confirming the suitability of the selected numerical methods, boundary conditions, and physical models, particularly for tube geometries involving complex flow and heat transfer mechanisms, such as serpentine tubes. In the present study, the model is validated by systematically comparing the simulated friction factor (f) and Nusselt number (Nu) for straight tubes without twisted tape inserts and serpentine tubes under representative flow conditions against well-established experimental data and classical empirical correlations available in the literature. Because publicly available experimental data for the composite configuration of serpentine tubes fitted with twisted tape inserts remain limited, the present validation primarily relies on classical correlations and previously published results. Nevertheless, the numerical predictions show good agreement with the reference data and are therefore considered capable of reliably capturing the flow and heat transfer characteristics of this type of structure. For straight tubes without twisted tape inserts under fully developed turbulent flow conditions, the Blasius and Gnielinski correlations were adopted as theoretical references for the friction factor, while the Dittus–Boelter correlation was used as the reference for the Nusselt number. A structured mesh was employed for the computational domain, and a mesh independence study was conducted to ensure that the (y+) value remained within the recommended range. Fig. 5 compares the predicted friction factor and Nusselt number as functions of Reynolds number with the corresponding values obtained from empirical correlations reported in the literature. The results show that, over the Reynolds number range of ($10{,}000 \leq Re \leq 22{,}000$), the average relative error of the friction factor is less than 4%, while the error in the Nusselt number remains within 5%, indicating that the numerical model provides satisfactory predictive accuracy.

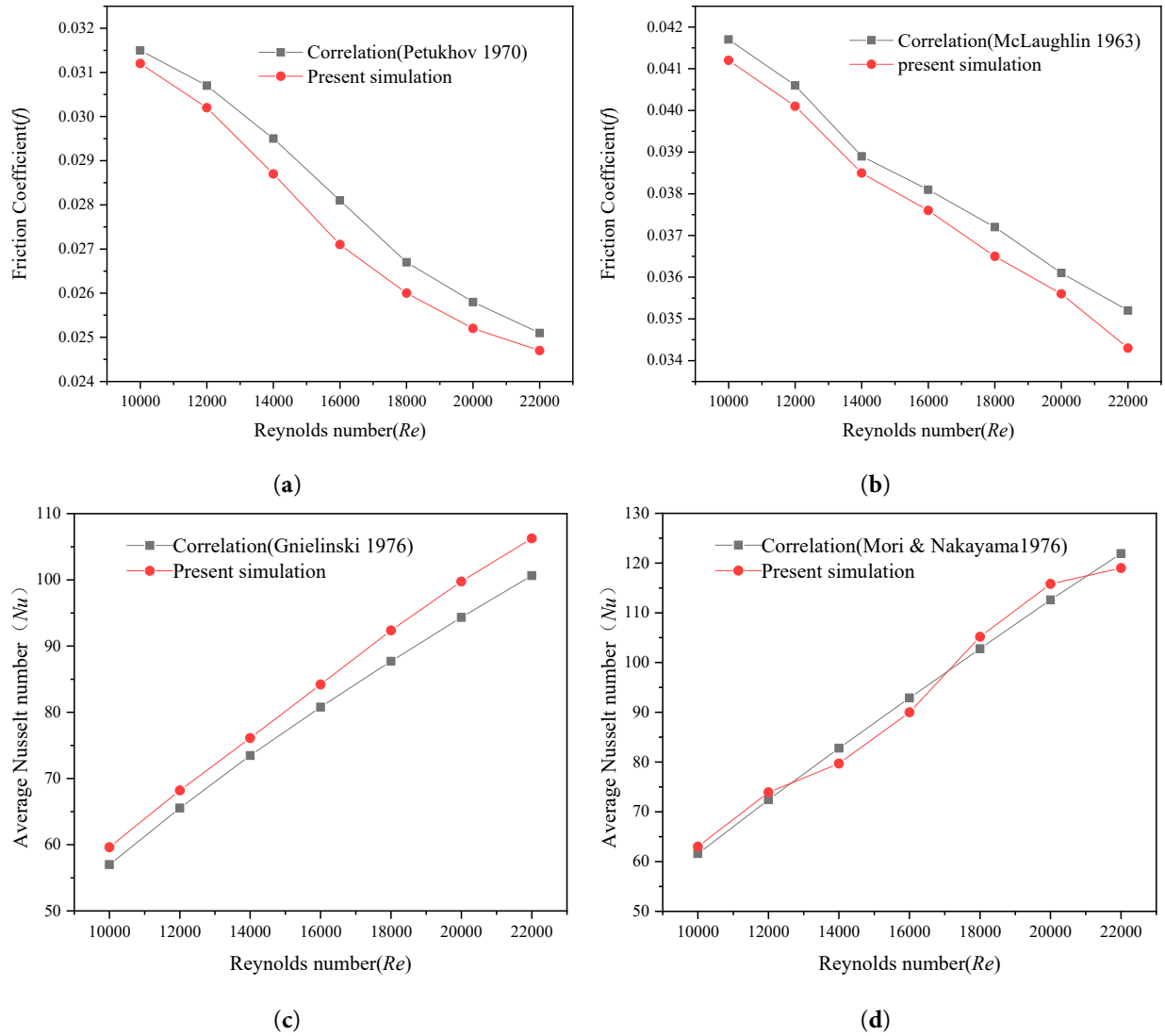

Figure 5: Comparison of current simulation results with literature. (**a**) Comparison of friction coefficients of straight pipe without twisted tape, (**b**) Comparison of friction coefficients of serpentine pipe without twisted tape, (**c**) Comparison of Nusselt numbers of straight pipe without twisted tape, (**d**) Comparison of Nusselt numbers of serpentine pipe without twisted tape.

4.2 Analysis of Limitations and Uncertainties in Numerical Methods

Although the numerical approach adopted in this study demonstrates satisfactory reliability in predicting flow and heat transfer characteristics in serpentine tubes, several limitations and sources of uncertainty remain, particularly in accurately capturing complex flow physics and ensuring robustness in engineering applications. The primary limitations of the numerical methodology are discussed as follows.

The Shear Stress Transport SST k-ω turbulence model employed in this study is known for its improved accuracy in near-wall regions and its capability to predict flow separation, making it suitable for a wide range of engineering applications. However, inherent limitations still exist. As a Reynolds-averaged Navier–Stokes (RANS)-based model, the SST k–ω formulation relies on time-averaged approximations of turbulent flow, which restricts its ability to resolve transient and anisotropic turbulence structures.

Consequently, complex unsteady flow features—such as the temporal evolution of coherent vortices and large-scale turbulent structures—may not be fully captured. In particular, under conditions involving strong flow unsteadiness or pronounced vortex dynamics, the predictive accuracy of the SST model may deteriorate, potentially leading to incomplete representation of the underlying physical mechanisms.

Despite the implementation of mesh independence studies and the adoption of sufficiently refined grids (approximately 2 million cells for the straight pipe model and 3.5 million cells for the serpentine pipe model), grid resolution continues to influence the numerical results. In particular, the accuracy of simulations in near-wall regions and flow separation zones remains sensitive to mesh refinement. Although structured meshes and systematic grid convergence tests were employed, discretization-related errors cannot be entirely eliminated. In addition, numerical simulations inherently introduce discretization and truncation errors, which may affect the prediction of key variables such as turbulence intensity, temperature distribution, and pressure gradients, thereby contributing to uncertainties in the evaluation of heat transfer performance and flow resistance.

Furthermore, the present study primarily relies on numerical simulations to analyze flow and heat transfer characteristics in serpentine tubes. Although the results have been compared with established empirical correlations, direct validation against experimental data is lacking. This limitation may introduce potential bias in the model predictions. In particular, under complex flow conditions—such as the coupling of swirl and secondary flows—and at high Reynolds numbers, the numerical model may not fully capture all relevant physical phenomena. Therefore, future work should incorporate experimental measurements to validate and further refine the proposed numerical framework.

4.3 Study on the Influence of Reynolds Number

The Reynolds number (*Re*), a key dimensionless parameter in fluid mechanics, reflects the relative magnitude of inertial and viscous forces during flow and directly influences the flow state (laminar versus turbulent) and heat transfer performance. In research on heat exchange equipment, systematically analyzing the patterns of flow and heat transfer behavior by adjusting the Reynolds number is a widely adopted scientific research method. This study focuses on serpentine and straight pipes, examining the influence of the Reynolds number on their friction coefficient (f) and mean Nusselt number (Nu). The friction coefficient (f) is used to characterize the resistance characteristics of fluid flow within a pipe (Darcy friction factor):

$$f = \frac{\Delta p \ d/L}{\frac{1}{2}\rho u^2} \tag{11}$$

Mean Nusselt number (Nu): Characterizes the ratio of convective heat transfer intensity to thermal conductivity intensity:

$$Nu = \frac{hd}{\lambda} \tag{12}$$

Average convective heat transfer coefficient (h):

$$h = \frac{q}{T_w - T_b} \tag{13}$$

where Δp is the pipe pressure drop, L is the pipe length, u is the average fluid velocity, ρ is the fluid density, h is the average convective heat transfer coefficient, λ is the fluid thermal conductivity, q is the wall heat flux density, T_w is the wall temperature, and T_b is the average fluid volume temperature.

While maintaining all other boundary conditions unchanged, seven inlet Reynolds numbers (*Re*) were considered, namely 10,000, 12,000, 14,000, 16,000, 18,000, 20,000, and 22,000. This range covers representative turbulent flow conditions and enables a systematic evaluation of the effects of Reynolds number on flow resistance and heat transfer performance. Fig. 6a,b presents the variations in the average Nusselt number (*Nu*) and friction factor (f) for different tube configurations with increasing Reynolds number. As *Re* increases from 10,000 to 22,000, the average Nusselt number of all serpentine and straight tube configurations increases significantly, whereas the friction factor decreases accordingly. This trend is consistent with the typical behavior of turbulent flow, in which higher flow intensity enhances convective heat transfer while reducing the relative contribution of viscous resistance. At a given Reynolds number, both the (*Nu*) and (f) values of the serpentine tubes are consistently higher than those of the straight tubes. This is attributed to the secondary flow induced by the curved geometry, which strengthens fluid mixing and heat transfer but also increases flow resistance. The insertion of twisted tapes further improves heat transfer performance by intensifying flow disturbance within the tube. Among the tested cases, the configuration with the smallest twist ratio (y = 5.77) yields the highest (*Nu*), although it also produces the largest (f). In contrast, larger twist ratios, such as (y = 12.48), provide a more favorable compromise between heat transfer enhancement and pressure loss. Overall, the combination of serpentine tubes and twisted tape inserts exhibits a clear synergistic effect on heat transfer enhancement. In particular, the serpentine tube fitted with a twisted tape of (y = 5.77) demonstrates the best heat transfer performance, albeit at the expense of the highest flow resistance. Therefore, in practical applications, the selection of geometric parameters should be based on a comprehensive consideration of heat transfer requirements and available pumping power.

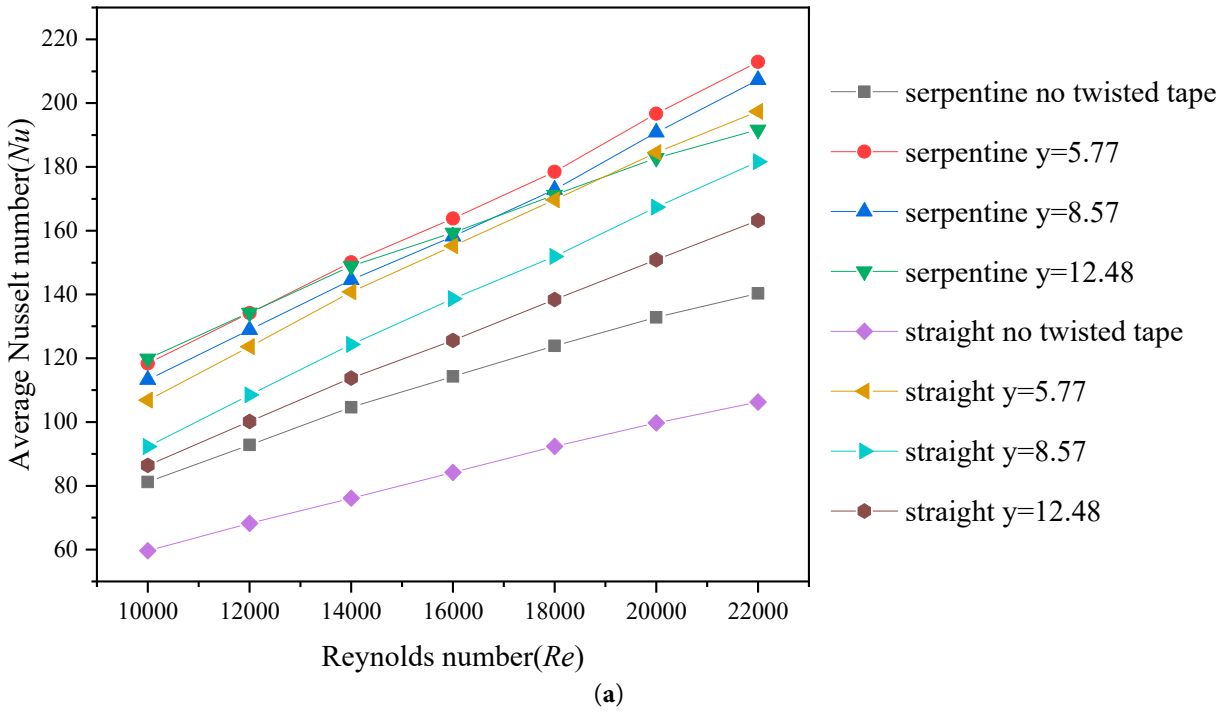

(**a**)

Figure 6: *Cont.*

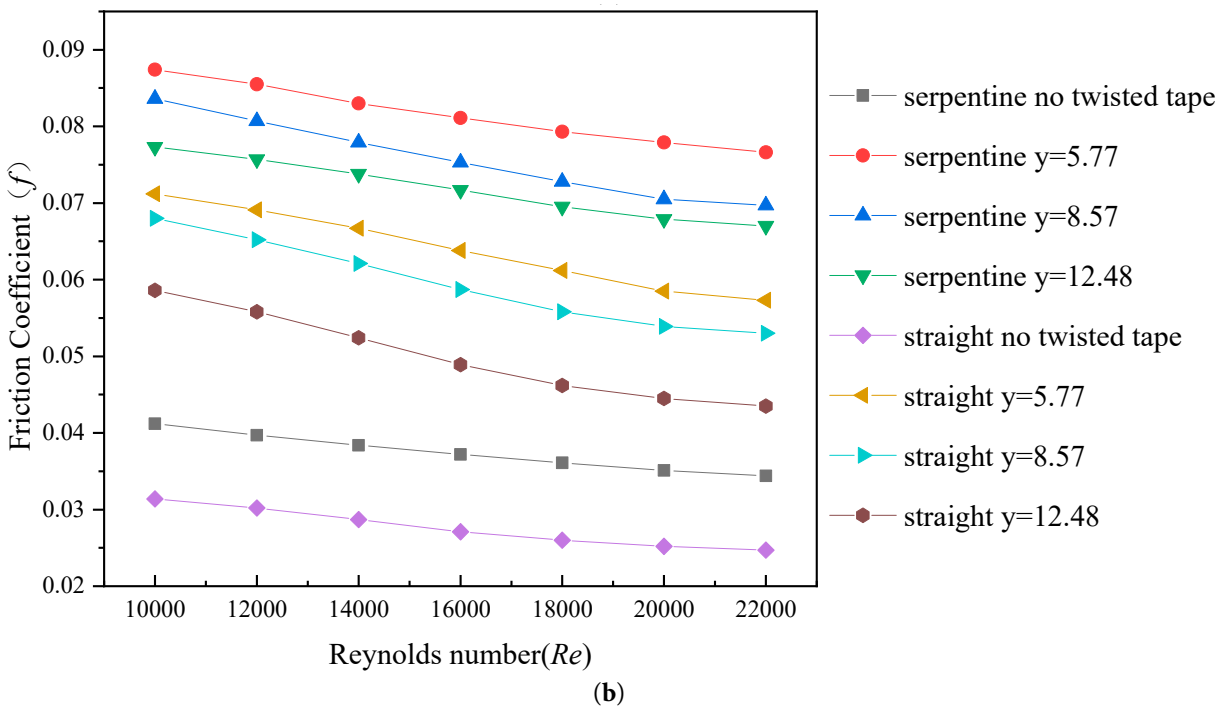

Figure 6: (**a**) shows the relationship between the average Nusselt number and the Reynolds number for various models. (**b**) shows the relationship between the friction coefficient and the Reynolds number.

4.4 Effect of Twist Ratio

The twist ratio is a key parameter affecting the performance of twisted tape inserts in pipes. Through their helical structure, twisted tapes induce rotational motion in the flowing fluid, thereby enhancing turbulence and disrupting the boundary layer. This leads to improved heat transfer, as well as enhanced scale prevention, mixing, and reaction processes. Such configurations are widely used in heat exchangers, chemical process piping, and fluid transport systems. Under conditions of an inlet Reynolds number of 10,000 and a constant wall temperature (T_w) of 293.15 K, four configurations were investigated: a straight pipe without twisted tape, a straight pipe with twisted tape, a serpentine pipe without twisted tape, and a serpentine pipe with twisted tape. The twist ratios of the inserts were 5.77, 8.57, and 12.48.

Visual analysis of the flow structure at a cross-section located 51.88 cm from the inlet shows that the insertion of twisted tape significantly alters the flow pattern and turbulence characteristics within the pipe due to its helical geometry. The twist ratio, as a key geometric parameter, plays a dominant role in governing this behavior. As illustrated by the axial velocity and streamline distributions in Fig. 7, the twisted tape induces a strong swirling flow structure by imposing circumferential shear on the fluid, thereby redistributing part of the axial kinetic energy into rotational motion. As the twist ratio decreases (from 12.48 to 5.77), the pitch of the tape shortens, resulting in intensified swirl strength, denser helical streamlines, a reduced rotation radius, and a significant increase in secondary flow intensity. In serpentine tubes, the centrifugal secondary flow generated by pipe curvature interacts with the forced swirling flow induced by the twisted tape, forming a superimposed flow structure that enhances flow three-dimensionality. This interaction leads to the formation of a high-velocity region along the outer side of the bend and a low-velocity region along the inner side, thereby increasing velocity non-uniformity. The enhanced secondary flow promotes radial transport by conveying fluid from the core region toward the near-wall region while simultaneously drawing heated fluid away from the wall toward the core, resulting in intensified radial and

circumferential mixing and providing a direct hydrodynamic mechanism for enhanced convective heat transfer. Furthermore, the axial velocity contours indicate that the presence of twisted tape transforms the cross-sectional velocity profile from the typical parabolic distribution of a smooth pipe to a fuller "M"-shaped or nearly uniform profile, accompanied by a significant increase in the near-wall velocity gradient. This, in turn, leads to increased wall shear stress, reflecting the enhanced frictional resistance. These observations are consistent with previous findings reported by Liaw et al. [31] and Kurnia et al. [32] on twisted-tape-enhanced heat transfer, further confirming the critical role of swirl structures in promoting turbulent mixing.

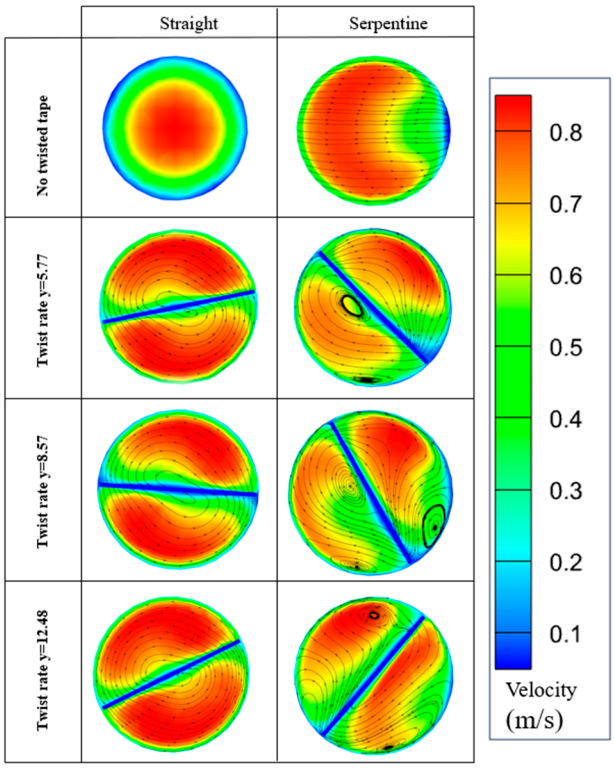

Figure 7: Axial velocity contours and streamline distributions of water flow at a cross-section located x = 51.88 cm from the inlet for different model configurations under Re = 10,000 and T_w = 293.15 K.

From the perspective of turbulent flow structure evolution, the distributions of turbulent kinetic energy (TKE), turbulence intensity, and turbulent viscosity shown in Figs. 8–10 collectively elucidate the mechanisms by which twisted tape enhances flow disturbances. The insertion of twisted tape modifies the flow path, and the strong shear generated between its edges and the channel wall induces flow separation and produces numerous vortical structures. The deformation, stretching, and breakdown of these vortices during downstream convection constitute the primary mechanisms for TKE production. As the twist ratio decreases, the combined effects of centrifugal forces and shear stresses intensify, leading to a significant increase in TKE generation. These enhanced energy fluctuations are further reflected in elevated turbulent viscosity levels, with high-viscosity regions extending asymmetrically from the tape surface toward the core of the flow. In serpentine tubes, curvature-induced pressure gradients further stretch and distort the vortical structures, promoting the development of a more fully established turbulent field. As a result, regions of high turbulent viscosity expand from the near-wall region to the entire cross-section of the bend,

indicating a transition from localized disturbance to global turbulent mixing. Turbulence intensity, as a dimensionless measure of flow fluctuation strength, further supports this trend, with high-intensity regions closely corresponding to zones of strong mixing and enhanced heat transfer potential. Meanwhile, the distribution of turbulent viscosity provides additional insight into the heat transfer enhancement mechanism from a transport perspective: regions of high turbulent viscosity coincide with areas of intense mixing, indicating that twisted tape effectively enhances turbulent diffusion, thins the thermal boundary layer near the wall, and ultimately leads to a substantial improvement in convective heat transfer performance.

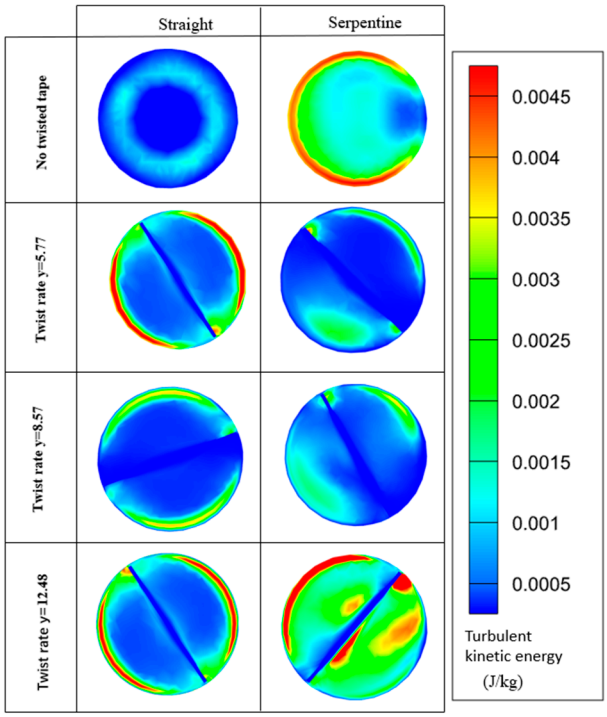

Figure 8: Turbulent kinetic energy contours of water flow at a cross-section located x = 51.88 cm from the inlet for different model configurations under Re = 10,000 and T_w = 293.15 K.

Analysis of the cross-sectional temperature field (Fig. 11) indicates that the combined use of twisted tape and serpentine tube geometry significantly enhances heat transport through the interaction between swirling flow and curvature-induced secondary flow. In a smooth straight tube, the thermal boundary layer gradually thickens along the flow direction, resulting in increased thermal resistance. The insertion of twisted tape induces strong swirling motion, which promotes effective radial mixing between the core region and the near-wall fluid. As the twist ratio decreases (from 12.48 to 5.77), the swirl intensity and turbulence level increase, leading to substantial disruption and thinning of the thermal boundary layer and producing a more uniform cross-sectional temperature distribution. In serpentine tubes, the Dean vortices generated by curvature interact with the swirl induced by the twisted tape, forming a more complex three-dimensional mixing structure that enables a transition from localized disturbance to global heat transfer enhancement. From a thermodynamic perspective, this confirms the superior capability of the combined configuration in improving energy transport efficiency.

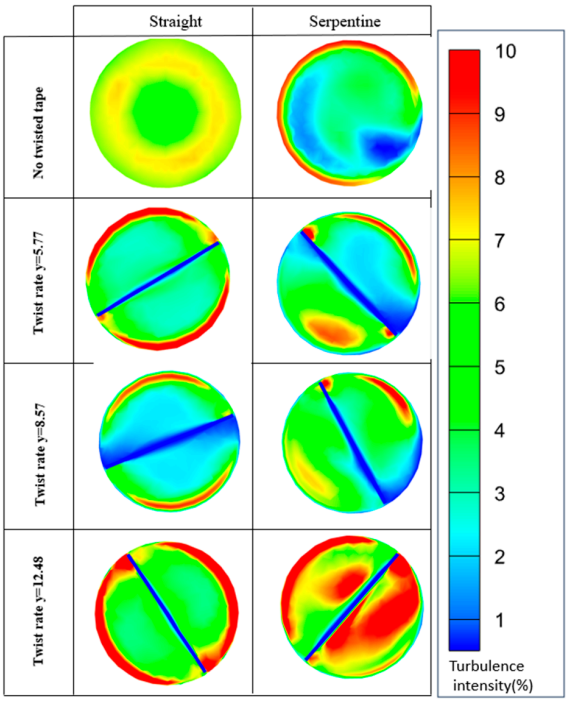

Figure 9: Turbulence intensity contours of water flow at a cross-section located x = 51.88 cm from the inlet for different model configurations under Re = 10,000 and T_w = 293.15 K.

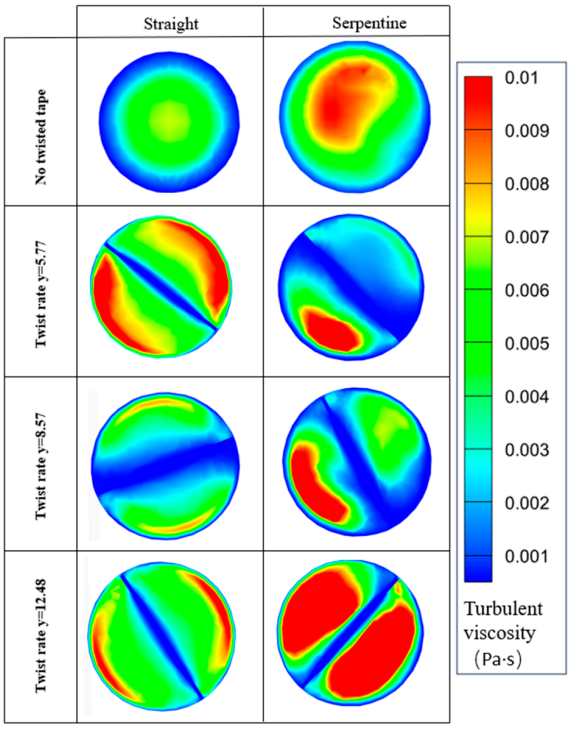

Figure 10: Turbulent viscosity contours of water flow at a cross-section located x = 51.88 cm from the inlet for different model configurations under Re = 10,000 and T_w = 293.15 K.

Based on the comprehensive analysis of Figs. 7–11, the heat transfer performance of different configurations can be ranked as follows. Under the same Reynolds number, the serpentine tube equipped with a low twist ratio twisted tape (y = 5.77) exhibits the highest heat transfer efficiency. This configuration fully exploits the synergy between curvature-induced secondary flow and forced swirling motion, resulting in dense helical streamlines, enhanced and widely distributed turbulent kinetic energy, turbulence intensity, and turbulent viscosity, and consequently strong radial mixing and global turbulence enhancement. These effects maximize the disruption of the thermal boundary layer and significantly promote heat diffusion. In contrast, a straight tube fitted with twisted tape enhances heat transfer through swirling flow but exhibits lower performance due to the absence of curvature-induced secondary flow. A serpentine tube without twisted tape relies solely on natural secondary flow, leading to limited enhancement. The smooth straight tube, with its relatively stable flow structure, exhibits the lowest heat transfer performance. In terms of the influence of twist ratio, for a given tube configuration, a lower twist ratio (smaller y value) results in more pronounced heat transfer enhancement, albeit at the cost of increased flow resistance.

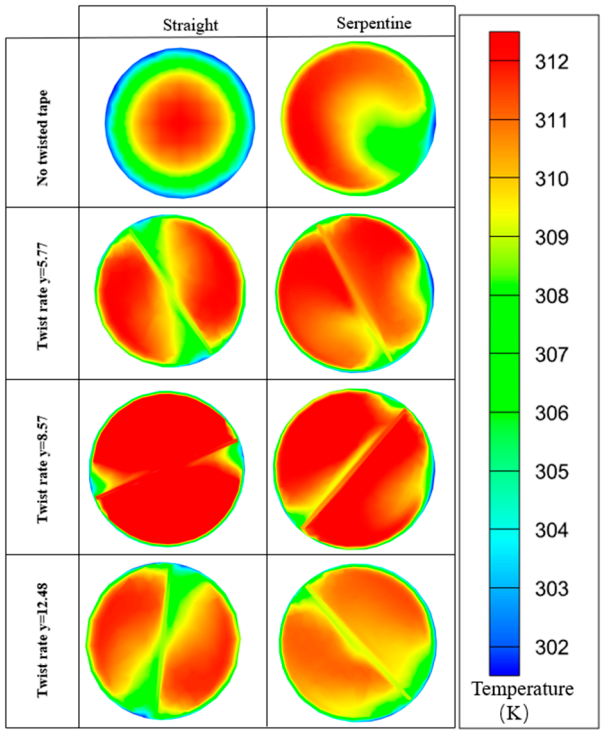

Figure 11: Temperature contours of water flow at a cross-section located x = 51.88 cm from the inlet for different model configurations under Re = 10,000 and T_w = 293.15 K.

4.5 Analysis of Flow Coupling and Turbulence Modulation Mechanisms

To further elucidate the fundamental mechanisms underlying heat transfer enhancement induced by twisted-tape inserts in serpentine tubes, a detailed analysis is conducted from the perspectives of flow structure evolution and turbulence transport. Particular emphasis is placed on swirl generation, the coupling between curvature-induced secondary flow and tape-induced vortices, as well as turbulence modulation and boundary layer disruption processes. The twisted tape continuously imposes circumferential shear on the fluid through its helical geometry, introducing a significant tangential velocity component into the

originally axial-dominated flow and thereby inducing a stable helical flow structure. From a momentum transport standpoint, this process represents a redistribution of axial momentum into angular momentum. As the twist ratio decreases, the rotational intensity per unit length increases, leading to stronger tangential forcing, higher vorticity, and enhanced mixing in both radial and circumferential directions.

In serpentine tubes, the curvature of the flow path gives rise to centrifugal forces that generate characteristic secondary flow structures, commonly referred to as Dean vortices. These vortices are manifested as transverse fluid migration from the inner wall to the outer wall, accompanied by recirculating flow loops driven by cross-sectional pressure gradients. When twisted-tape inserts are introduced, the forced swirl interacts with the curvature-induced secondary flow, resulting in a spatial superposition that produces a more complex three-dimensional vortex system. This coupling effect not only intensifies multidirectional fluid mixing in the axial, radial, and circumferential directions, but also significantly broadens the spatial distribution of regions with high turbulent kinetic energy. As a result, the flow transitions from localized perturbations to globally intensified turbulence, establishing more efficient pathways for heat transport.

From the perspective of turbulence modulation, the combined effects of twisted-tape-induced swirl and channel curvature substantially enhance velocity gradients and shear interactions within the flow. This promotes the generation, breakdown, and cascade of vortical structures, leading to elevated turbulent kinetic energy and turbulent viscosity levels. The resulting enhancement in turbulent transport shifts the dominant heat transfer mechanism from molecular conduction toward turbulent convective diffusion. Meanwhile, the interaction between swirl flow and secondary flow continuously disturbs the thermal boundary layer, frequently inducing local thinning or partial separation. Consequently, the thermal boundary layer, which would otherwise grow along the axial direction, is periodically disrupted and regenerated. High-temperature fluid near the wall is continuously transported into the core region, while cooler bulk fluid replenishes the near-wall region, thereby significantly reducing thermal resistance and enhancing convective heat transfer.

Overall, the combined configuration of serpentine tubes and twisted-tape inserts achieves a fundamental reorganization of flow structures and heat transport pathways through the synergistic effects of swirl induction, secondary flow enhancement, and turbulence modulation. The enhanced heat transfer performance is achieved at the expense of increased flow resistance, reflecting an intrinsic trade-off between heat transfer augmentation and energy dissipation. This mechanistic understanding provides a clear explanation for the simultaneous increase in both Nusselt number and friction factor observed in such systems.

4.6 Entropy Generation Analysis

To further evaluate the impact of twisted-tape inserts on the heat transfer performance of serpentine tubes from a second-law thermodynamics perspective, an entropy generation analysis is conducted. Entropy generation reflects the degree of irreversibility within the system, primarily arising from heat transfer driven by temperature gradients and viscous dissipation associated with fluid friction. Accordingly, the total entropy generation rate can be expressed as follows:

$$S_{gen} = S_{gen,T} + S_{gen,F} \tag{14}$$

here, $S_{gen,T}$ denotes the thermal entropy generation rate, and $S_{gen,F}$ denotes the frictional entropy generation rate.

Due to the presence of temperature gradients within the fluid, irreversible losses occur during the heat transfer process; its local entropy generation rate can be expressed as:

$$S_{gen,T} = \frac{k}{T^2}\left[\left(\frac{\partial T}{\partial x}\right)^2 + \left(\frac{\partial T}{\partial y}\right)^2 + \left(\frac{\partial T}{\partial z}\right)^2\right] \tag{15}$$

here, k is the thermal conductivity of the fluid, and T is the local temperature.

During the flow of a fluid within a pipe, viscous effects generate shear stress and lead to the dissipation of mechanical energy; the corresponding entropy generation rate is:

$$S_{gen,F} = \frac{\mu}{T}\Phi \tag{16}$$

Fig. 12 presents the variations of frictional entropy generation and thermal entropy generation under different structural configurations and Reynolds numbers. As shown in Fig. 12a, frictional entropy generation increases markedly with increasing Reynolds number, and this trend is further intensified by the introduction of twisted tape inserts, especially at lower twist ratios (y = 5.77), which is mainly attributed to the combined effects of swirl flow induced by the twisted tape and curvature-induced secondary flow in the serpentine tube, leading to enhanced velocity gradients and increased turbulent dissipation. As illustrated in Fig. 12b, thermal entropy generation also exhibits an increasing trend with Reynolds number, although its growth rate is relatively moderate compared to that of frictional entropy generation, and this behavior can be explained by the intensified convective heat transfer at higher flow velocities, which enhances energy transport while simultaneously increasing thermal irreversibility; meanwhile, the presence of twisted tape inserts and serpentine geometry promotes radial fluid mixing and modifies the temperature field, slightly affecting the magnitude of thermal entropy generation without altering its overall increasing tendency. Overall, heat transfer enhancement in the present configuration is accompanied by simultaneous increases in both frictional and thermal entropy generation, indicating an inherent trade-off between improved heat transfer performance and increased energy dissipation.

Fig. 13 further illustrates the relative contributions of thermal entropy generation and frictional entropy generation under varying Reynolds number conditions. The results show that at low Reynolds numbers, irreversible losses are predominantly governed by thermal entropy generation, whereas with increasing Reynolds number, the contribution of frictional entropy generation progressively increases, indicating a transition in the dominant irreversibility mechanism from heat-transfer-driven to flow-dissipation-dominated behavior. Moreover, the incorporation of serpentine geometry and twisted tape inserts significantly enhances the proportion of frictional entropy generation, particularly at lower twist ratios. This finding suggests that the fundamental mechanism of heat transfer enhancement lies in the intensification of flow disturbance and shear effects, whereby improved heat transport performance is achieved at the expense of increased flow dissipation, ultimately leading to an overall enhancement in thermo-hydraulic performance.

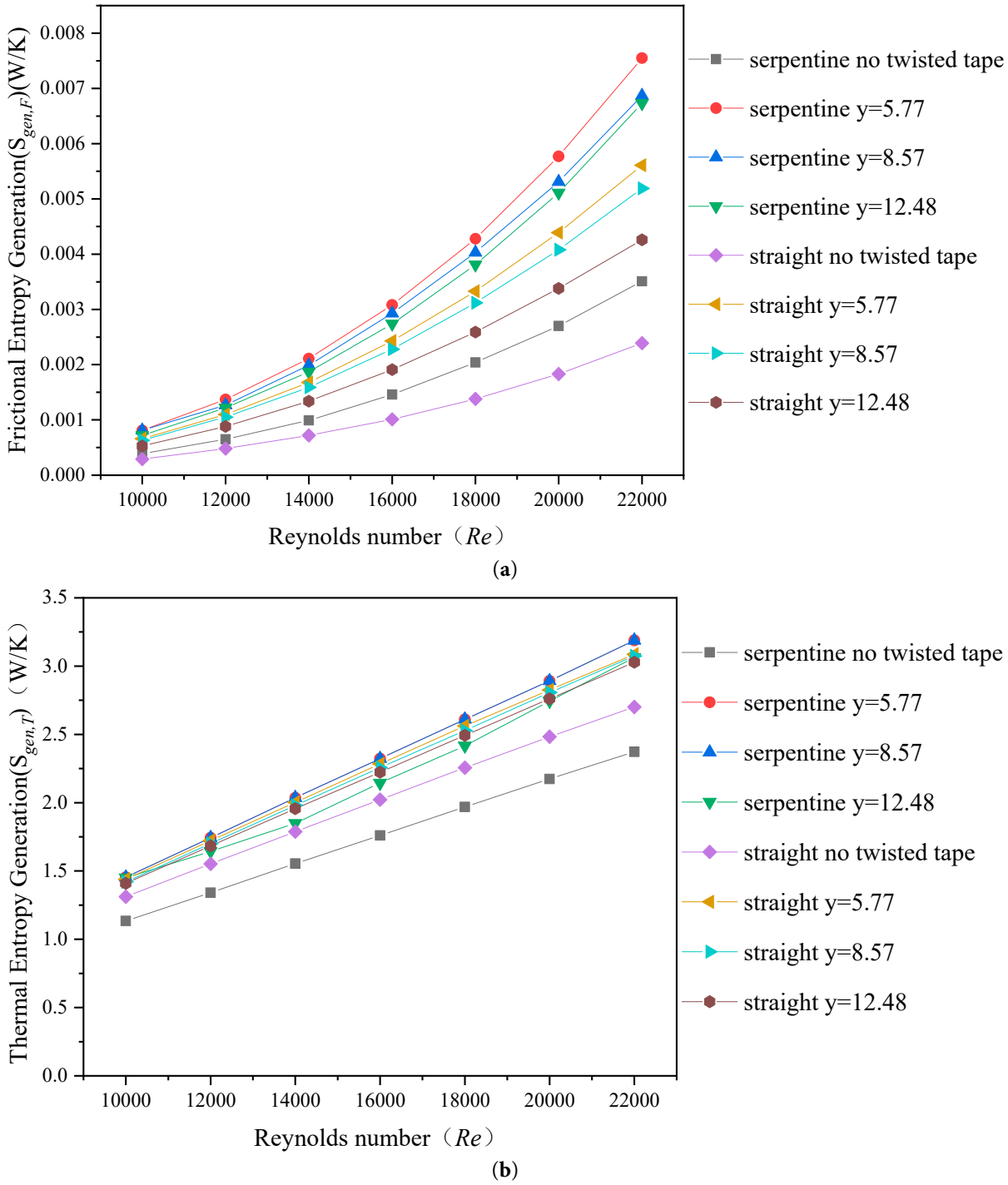

Figure 12: Characteristic curves of (**a**) frictional entropy generation and (**b**) thermal entropy generation under different Reynolds numbers and structural configurations.

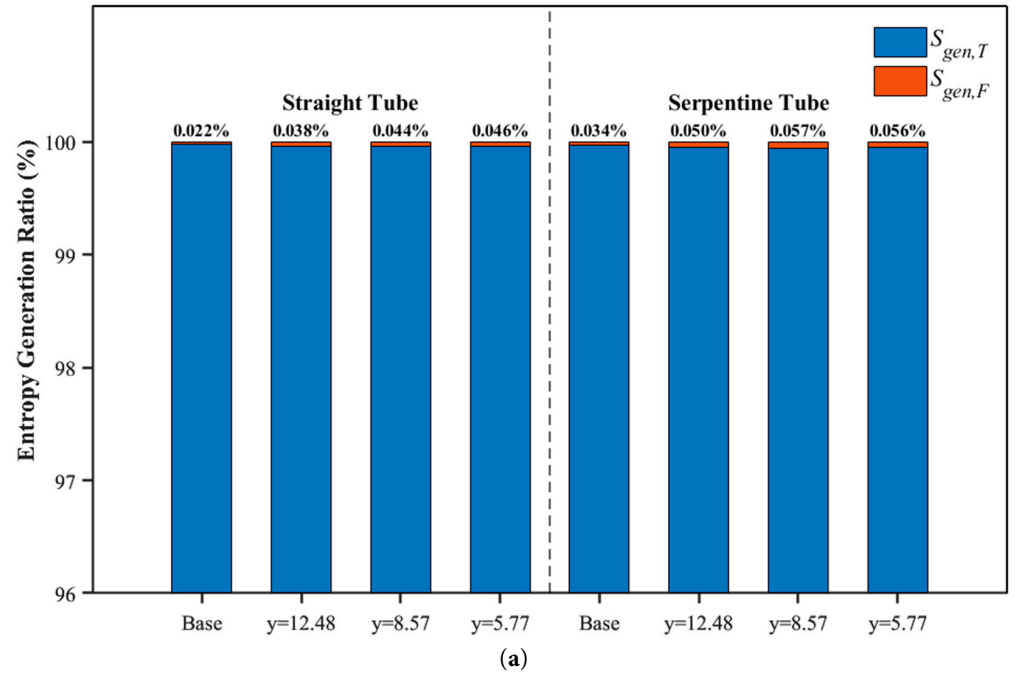

(a)

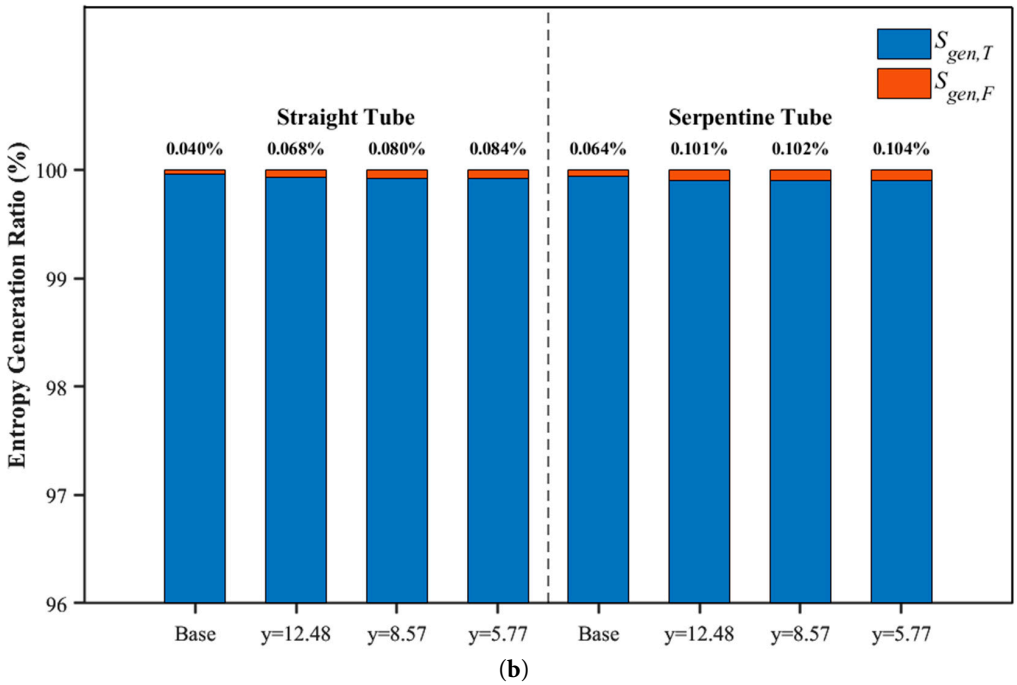

(b)

Figure 13: *Cont.*

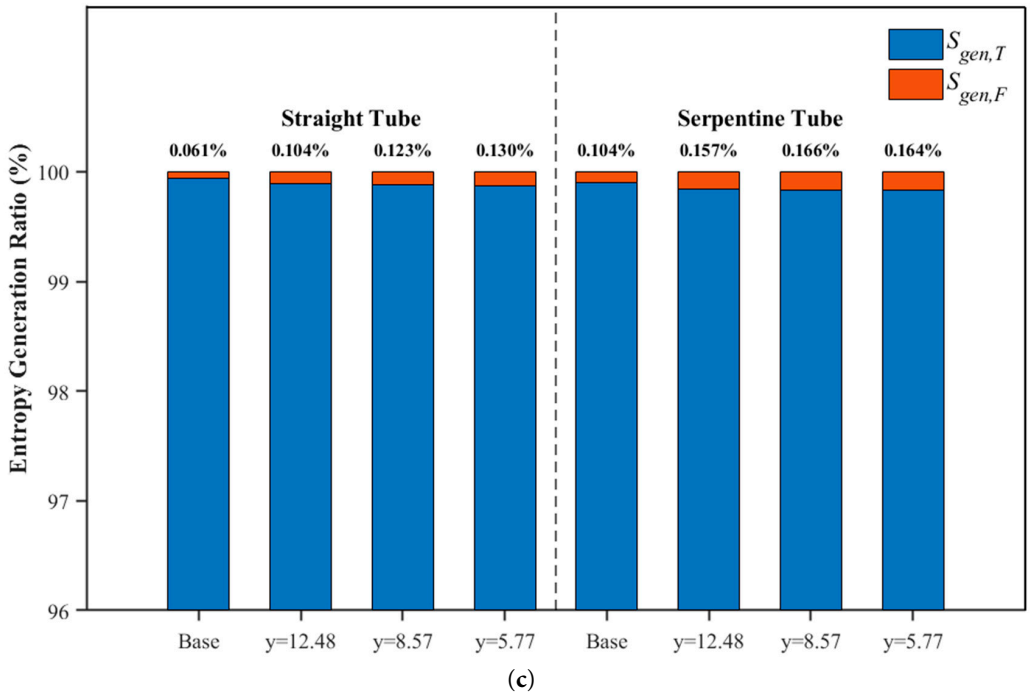

(**c**)

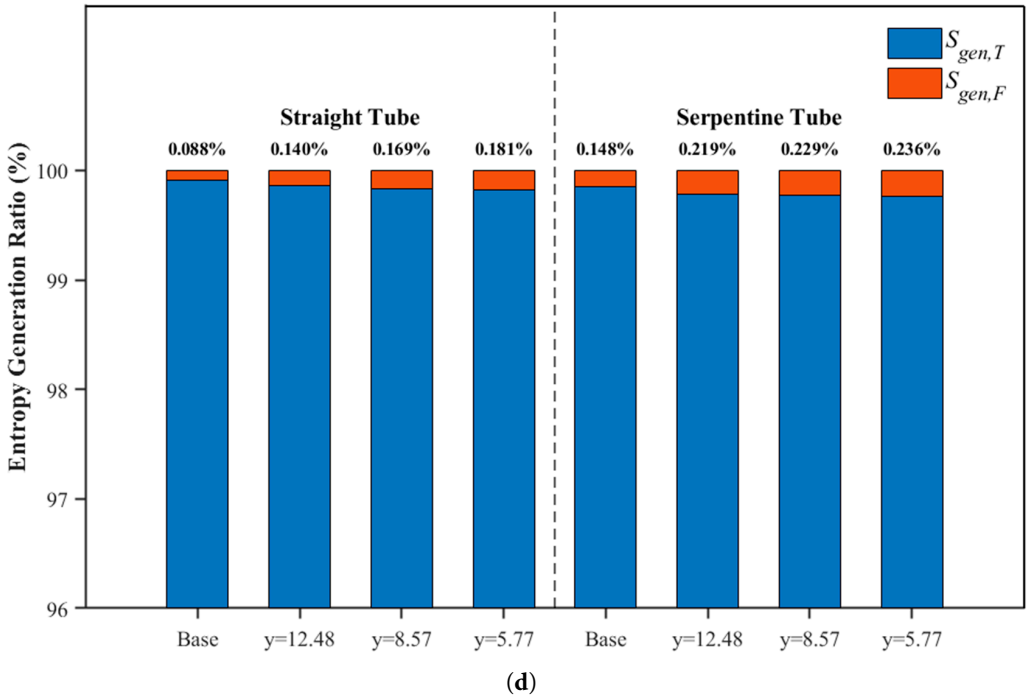

(**d**)

Figure 13: Relative contributions of entropy generation at different Reynolds numbers: (**a**) *Re* = 10,000; (**b**) *Re* = 14,000; (**c**) *Re* = 18,000; (**d**) *Re* = 22,000.

To examine the spatial evolution of entropy generation along the axial flow direction, several representative cross-sections were selected from the inlet to the outlet. Fig. 14a shows the contour distribution of total entropy generation in the straight tube, while Fig. 14b presents the corresponding distributions at different axial positions in the serpentine tube. Overall, entropy generation is primarily concentrated near the tube wall and in the vicinity of the twisted tape, indicating that irreversible losses

are mainly governed by the combined effects of temperature and velocity gradients. In the smooth straight tube, the entropy generation distribution exhibits a relatively uniform annular pattern, with high-value regions concentrated in the near-wall zone due to the coexistence of strong temperature and velocity gradients, where heat transfer–induced entropy generation dominates while the contribution from flow friction remains relatively small. After the insertion of twisted tape, the entropy generation distribution is significantly altered, and a high-entropy-generation band aligned with the tape geometry emerges in the central region, forming a distinct diagonal or helical structure. This behavior is attributed to the swirl induced by the twisted tape, which enhances velocity shear and turbulent mixing, thereby increasing viscous dissipation and significantly elevating frictional entropy generation. Meanwhile, the enhanced radial mixing driven by the swirling flow causes the high-entropy-generation regions to extend from the wall toward the core of the flow, and along the axial direction, the entropy generation distribution evolves progressively from the entrance region toward a fully developed state, reflecting the gradual establishment of the coupled thermal and hydrodynamic fields.

In the inlet region, where the flow is not yet fully developed, the entropy generation distribution is highly non-uniform and exhibits pronounced local fluctuations. As the fluid progresses downstream, the flow structure gradually stabilizes, and the entropy generation field becomes more regular, with high-value regions primarily concentrated near the tube wall and the inserted elements. In serpentine tubes, curvature-induced centrifugal forces generate secondary flows within the cross-section, leading to a redistribution of velocity and temperature fields and resulting in a distinctly asymmetric entropy generation pattern. In general, the outer side of the bend exhibits significantly higher entropy generation than the inner side due to stronger velocity and temperature gradients, indicating that while curvature enhances fluid mixing, it also increases local irreversible losses. When twisted-tape inserts are introduced into the serpentine tube, the entropy generation distribution becomes more complex. The swirl induced by the inserts interacts with the curvature-driven secondary flow, producing a strongly three-dimensional flow field in which high-entropy-generation regions exhibit a helical distribution across the cross-section. This coupling enhances radial and circumferential mixing and intensifies heat transport, but at the same time increases flow resistance and energy dissipation.

From an engineering perspective, entropy generation analysis provides valuable guidance for the optimal design of enhanced heat transfer structures. The results indicate that while the combined use of twisted-tape inserts and serpentine tubes can significantly reduce thermal entropy generation and improve heat transfer performance through enhanced turbulent mixing, it also increases frictional entropy generation, leading to higher flow resistance and energy consumption. Therefore, practical design requires a balance between heat transfer enhancement and energy dissipation, depending on specific application requirements. For instance, in compact heat exchangers and waste heat recovery systems, configurations with lower twist ratios are preferable to achieve higher heat transfer efficiency, whereas in energy-sensitive systems, higher twist ratios are more suitable for reducing pressure drop and associated energy losses. These findings provide a clear theoretical basis for the application and optimization of serpentine-tube-based heat transfer enhancement structures in energy and process engineering systems.

Overall, the entropy generation results are consistent with the previously observed temperature field and turbulence characteristics. The inserts improve heat transfer by strengthening turbulent mixing and shear effects, while also increasing system irreversibility, and the serpentine geometry further amplifies this behavior. These findings confirm that heat transfer enhancement is fundamentally governed by a trade-off between improved heat transfer performance and increased irreversible losses.

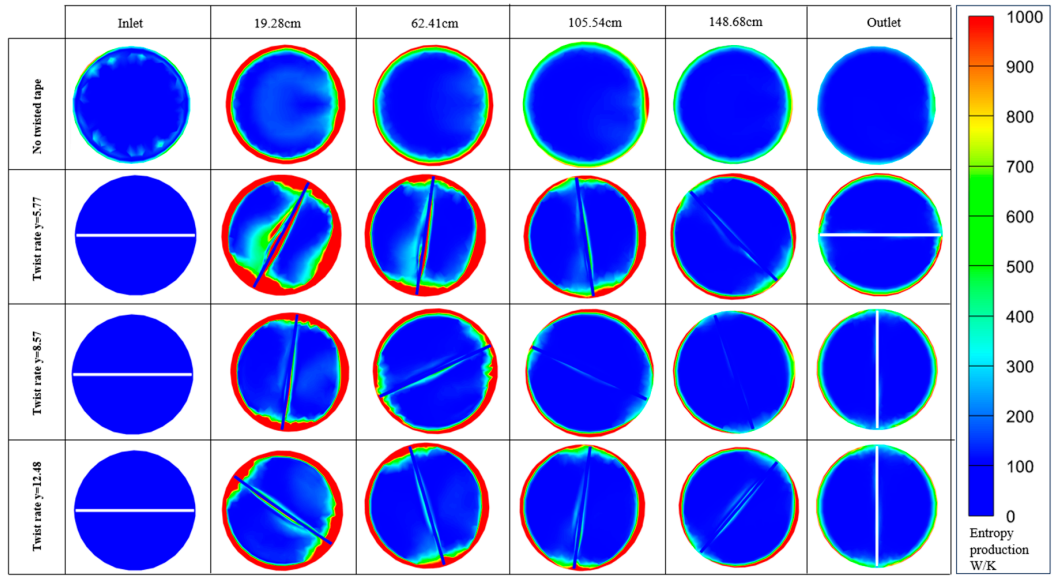

(**a**)

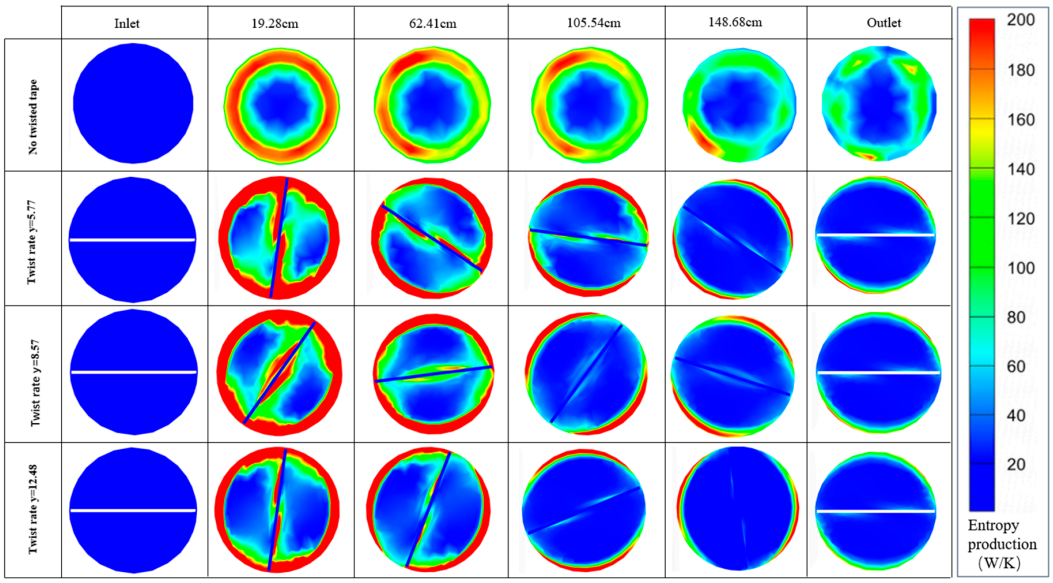

(**b**)

Figure 14: Total entropy generation distributions of water flow across different pipe cross-sections for (**a**) a straight pipe and (**b**) a serpentine pipe under Re = 10,000 and T_w = 293.15 K.

4.7 Performance Indicators

To quantitatively evaluate the effect of twisted-tape inserts on the overall thermohydraulic performance of serpentine tubes, while accounting for the additional flow resistance associated with heat transfer enhancement, the performance evaluation criterion (PEC) is employed. This metric compares the heat transfer performance of enhanced tubes with that of a reference smooth straight tube under identical pumping power conditions and is defined as follows:

$$\mathrm{PEC} = \frac{Nu/Nu_0}{(f/f_0)^{1/3}} \tag{17}$$

Furthermore, to intuitively and quantitatively assess the "benefits" and "costs" associated with enhanced heat transfer techniques, this paper introduces the Heat Transfer Enhancement Ratio (R_{Nu}) and the Drag Penalty Ratio (R_f) as evaluation parameters. Their definitions are as follows:

$$R_{Nu} = \frac{Nu}{Nu_0},\ R_f = \frac{f}{f_0} \tag{18}$$

where: PEC: Performance Evaluation Criterion (a value greater than 1 indicates performance enhancement); Nu: Nusselt number of the enhanced tube; Nu_0: Nusselt number of the reference smooth tube; f: Friction factor of the enhanced tube (Darcy friction factor); f_0: Friction factor of the reference tube (Darcy friction factor).

Based on the intrinsic mechanisms of thermodynamics and fluid dynamics, an analysis of Fig. 15a,b reveals that—although the numerical increase in the drag coefficient typically exceeds that of the heat transfer coefficient—a cross-reference with Table 3 demonstrates that the comprehensive performance evaluation criterion (PEC) value remains above 1. Fundamentally, this reflects the enhancement in energy transport efficiency achieved through the optimization of the flow field structure. Under the constraint of constant pumping power—given that pumping power is proportional to the cube of the flow velocity—a moderate reduction in flow velocity is sufficient to offset the negative impact resulting from the significant increase in the friction coefficient. Concurrently, the secondary flows and Dean vortices synergistically induced by the twisted tape and the serpentine tube establish ordered radial mixing channels, thereby achieving the effective disruption of the thermal boundary layer. This reconstruction of the flow field structure enables the fluid to exchange a higher rate of mechanical energy dissipation (i.e., the "cost" represented by flow resistance) for significantly enhanced heat transport capability (i.e., the "benefit" represented by heat transfer effectiveness), thereby realizing a net gain in overall thermo-hydraulic performance.

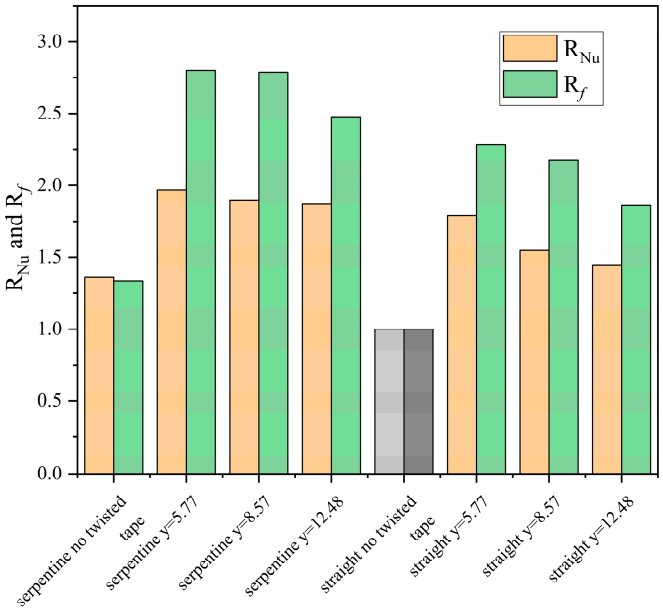

(**a**)

Figure 15: *Cont.*

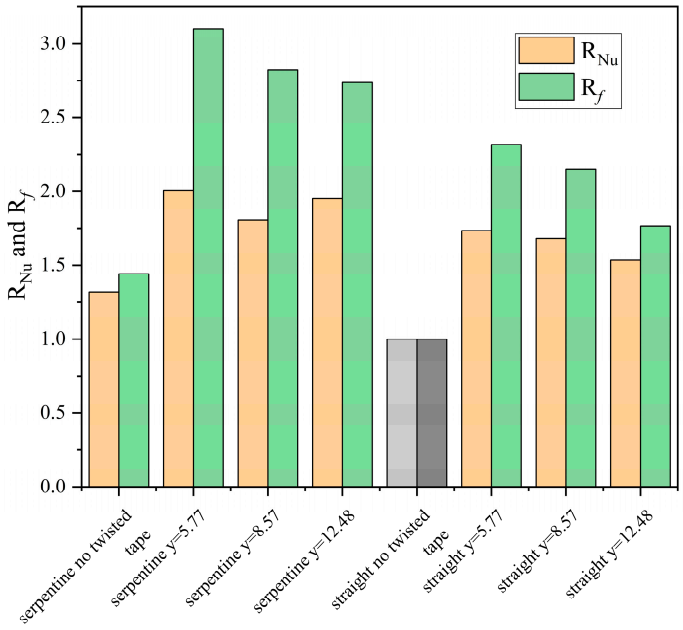

(**b**)

Figure 15: A comparison of the heat transfer enhancement ratio (R_{Nu}) and the friction penalty ratio (R_f) at different Reynolds numbers using bar charts. Specifically, (**a**) shows the results at Re = 10,000, while (**b**) shows the results at Re = 22,000.

Table 3: Comprehensive Performance Evaluation Indicators (PEC) for Various Configurations.

Re	Smooth Straight Tube	Serpentine Tape	Straight y = 5.77	Serpentine y = 5.77	Straight y = 8.57	Serpentine y = 8.57	Straight y = 12.48	Serpentine y = 12.48
10,000	1	1.236	1.361	1.396	1.194	1.349	1.178	1.367
12,000	1	1.233	1.377	1.391	1.227	1.362	1.197	1.388
14,000	1	1.242	1.368	1.384	1.256	1.375	1.217	1.380
16,000	1	1.205	1.383	1.350	1.261	1.340	1.210	1.350
18,000	1	1.186	1.376	1.333	1.258	1.306	1.218	1.339
20,000	1	1.177	1.327	1.354	1.291	1.293	1.238	1.365
22,000	1	1.169	1.310	1.374	1.304	1.277	1.271	1.373

Through a systematic analysis of the performance evaluation criterion (PEC), this study clarifies the thermohydraulic characteristics of different structural configurations. Among the geometries considered, serpentine tubes consistently exhibit higher PEC values than straight tubes, highlighting the synergistic interaction between curvature-induced secondary flow and the swirl generated by twisted tape. Under all operating conditions, the PEC values range from 1.17 to 1.396, with the optimal configuration depending on the Reynolds number. At low Reynolds numbers ($Re \leq$ 12,000), twisted tapes with low twist ratios (y = 5.77) induce stronger swirl and turbulence, promoting more effective fluid mixing and yielding superior overall performance; for example, at Re = 10,000, the serpentine tube with y = 5.77 achieves a maximum PEC value of 1.396. As the Reynolds number increases, inertial effects become more pronounced and turbulence develops more fully; under these conditions, excessively strong swirl leads to increased flow resistance, thereby reducing the performance advantage of low-twist-ratio configurations. At higher Reynolds numbers ($Re \geq$ 20,000), larger twist ratios (y = 12.48) provide a better balance between heat transfer enhancement

and flow resistance, resulting in more stable overall performance; for instance, at Re = 22,000, the serpentine tube with y = 12.48 achieves a PEC value of 1.373. From an engineering perspective, these results indicate that low twist ratios are preferable under low Reynolds number conditions to maximize heat transfer enhancement, whereas higher twist ratios are more suitable at high Reynolds numbers to achieve an optimal balance between heat transfer and pressure drop.

From the perspective of overall thermohydraulic performance, the optimal balance between heat transfer enhancement and pressure drop in serpentine configurations is strongly dependent on flow conditions and geometric parameters. At low Reynolds numbers, configurations with low twist ratios significantly enhance heat transfer by promoting swirl-induced mixing and turbulence, with the resulting heat transfer gains outweighing the associated drag penalty. In contrast, at high Reynolds numbers, where the flow is already highly turbulent, excessive swirl leads to additional energy dissipation; under such conditions, configurations with moderate to high twist ratios exhibit more favorable overall performance by achieving a better compromise between heat transfer and pressure drop. Furthermore, the interaction between curvature-induced secondary flow and swirl generated by the twisted tape exhibits both synergistic and competitive characteristics. At low twist ratios, swirl dominates and strongly couples with secondary flow, forming an intense three-dimensional mixing structure. As the twist ratio increases, the swirl effect weakens, and curvature-induced secondary flow gradually becomes dominant, resulting in a more stable flow field but reduced mixing intensity. This transition in the governing mechanism provides the fundamental physical basis for the observed variations in heat transfer performance and flow resistance.

4.8 Flow and Heat Transfer Correlations

The significance of numerical simulations lies not only in revealing flow mechanisms and heat transfer characteristics, but also in developing predictive tools with practical engineering applicability. Based on the simulation results, a semi-empirical correlation in the form of a power-law function is established for serpentine tubes fitted with twisted tapes. Considering the effects of Reynolds number (Re) and twist ratio (y), the correlation is expressed as follows:

$$Nu = CRe^{a}y^{b},\ f = C_{f}Re^{m}y^{n} \tag{19}$$

By performing a log-linear regression on the simulated data within the ranges $10{,}000 \leq Re \leq 22{,}000$ and $5.77 \leq y \leq 12.48$, the following results were obtained:

$$Nu = 0.153Re^{0.730}y^{-0.049} \tag{20}$$

$$f = 0.731Re^{-0.201}y^{-0.148} \tag{21}$$

The fitting results show that the proposed correlations can reliably predict the heat transfer and flow resistance characteristics of serpentine tubes with inserts within the investigated parameter range, with average relative errors of approximately 4.6% for the Nusselt number (Nu) and 5.1% for the friction factor (f). These results provide a concise and reliable quantitative basis for the design and performance prediction of similar heat transfer enhancement systems. It should be noted that the above relationship applies only to serpentine tube-inserted twisted tape inserts within the parameter range used in this study ($10{,}000 \leq Re \leq 22{,}000$, $5.77 \leq y \leq 12.48$); caution should be exercised when applying it to other flow conditions or geometric parameters.

5 Conclusion

(1) Effect of serpentine geometry on heat transfer and flow resistance

Compared with straight tubes, serpentine tubes significantly enhance heat transfer due to curvature-induced secondary flow, which promotes radial mixing and leads to higher Nusselt numbers. However, this enhancement is accompanied by increased flow resistance, reflecting an inherent trade-off between heat transfer improvement and pressure drop.

(2) Enhancement mechanism of twisted tape inserts

Twisted tape inserts induce strong swirl flow and intensify turbulence, continuously disturbing and locally disrupting the thermal boundary layer, thereby enhancing convective heat transfer. At the same time, increased velocity gradients and shear stresses lead to higher flow resistance. This mechanism is governed by the combined effects of swirl generation, turbulence modulation, and boundary layer disruption.

(3) Influence of twist ratio on thermohydraulic performance

The twist ratio plays a key role in determining heat transfer enhancement and flow resistance. A low twist ratio (y = 5.77) generates stronger swirl and turbulence, resulting in maximum heat transfer enhancement but also the highest pressure drop. In contrast, a high twist ratio (y = 12.48) produces weaker disturbances, leading to moderate heat transfer enhancement with reduced flow resistance. These results indicate that decreasing the twist ratio improves heat transfer at the expense of increased energy dissipation.

(4) Comprehensive performance evaluation and optimal configurations

The performance evaluation criterion (PEC) shows that all enhanced configurations achieve PEC values greater than 1 (approximately 1.17–1.396), confirming improved overall performance. A clear synergistic effect is observed when serpentine tubes are combined with twisted tape inserts. The optimal configuration depends on the Reynolds number: at low Reynolds numbers ($Re \leq 12{,}000$), the best performance is obtained at y = 5.77 (PEC up to 1.396), whereas at high Reynolds numbers ($Re \geq 20{,}000$), a larger twist ratio (y = 12.48) provides a better balance between heat transfer enhancement and pressure drop (PEC $\approx$ 1.373).

(5) Thermodynamic interpretation based on entropy generation analysis

Entropy generation analysis indicates that system irreversibility arises from the combined effects of thermal and frictional entropy generation. The interaction between swirl flow and secondary flow enhances mixing and reduces temperature gradients, which reduces local temperature gradients; however, the overall thermal entropy generation may still increase with Reynolds number due to intensified convective heat transfer. Increased velocity gradients and turbulent dissipation lead to higher frictional entropy generation. Overall, heat transfer enhancement can be understood as a trade-off between improved heat transport and increased irreversible losses.

(6) Engineering implications

The present results provide practical guidance for the design of enhanced heat transfer systems. A low twist ratio is recommended when heat transfer enhancement is the primary objective, whereas a higher twist ratio is preferable for systems requiring lower pressure drop and reduced pumping power. The combined use of serpentine tubes and twisted tape inserts is particularly promising for compact heat exchangers, waste heat recovery systems, and thermal management applications.

Acknowledgement: We acknowledged the support of the National Key Research and Development Program of China, the National Natural Science Foundation of China, the Central Guidance on Local Scientific and Technological Development Funds and the Yunnan Fundamental Research Projects.

Funding Statement: This research was funded by the National Key Research and Development Program of China (grant number 2022YFC3902000), the National Natural Science Foundation of China (grant number 52166004), the Central Guidance on Local Scientific and Technological Development Funds (grant number 202407AB110022), and the Yunnan Fundamental Research Projects (grant number 202501AS070131).

Author Contributions: Conghai Chen: survey, methodology, data organization, validation, writing—original manuscript. Dingran Sun: methodology. Yikai Chen: investigation. Jianxin Xu: supervision, writing—review and editing. Hua Wang: supervision, guidance. All authors reviewed and approved the final version of the manuscript.

Availability of Data and Materials: The datasets generated and analyzed during the current study are not publicly available due to confidentiality request by the party providing the data but are available from the corresponding author on reasonable request.

Ethics Approval: Not applicable.

Conflicts of Interest: The authors declare no conflicts of interest.

Abbreviations

Table of Variable Symbols

Symbol	Meaning	Units
b	Characteristic width of the twisted tape	(m)
c_p	Specific heat capacity	J/(kg·K)
d	Inner diameter of the tube	(m)
D	Tube diameter	(m)
F	Volumetric force density	(N/m^3)
f	Friction factor	(-)
f_0	Friction factor of the reference straight tube	(-)
g	Gravitational acceleration	(m/s^2)
h	Average convective heat transfer coefficient	W/(m^2·K)
H	Axial length for a 180° twist of the tape	(m)
L	Tube length	(m)
Nu_0	Nusselt number of the reference straight tube	(-)
Nu	Average Nusselt number	(-)
p	Pressure	(Pa)
Δp	Pressure drop	(Pa)
P_k	Turbulent kinetic energy production term	kg/(m·s^3)
q	Wall heat flux	(W/m^2)
Re	Reynolds number	(-)
R_{Nu}	Heat transfer enhancement ratio	(-)
R_f	Friction penalty ratio	(-)
T_w	Wall temperature	(K)
T_b	Bulk mean fluid temperature	(K)
y	Twist ratio	(-)
Φ	Viscous dissipation term	(W/m^3)
ω	Specific dissipation rate	(s^{-1})
τ	Stress tensor	(Pa)
ρ	Density of water	(kg/m^3)
μ	Dynamic viscosity	(kg/(m·s))
λ	Thermal conductivity	(W/(m·K))

κ	Turbulent kinetic energy	(m^2/s^2)
u	Velocity vector	(m/s)
S	Strain rate tensor	(s^{-1})
μ_t	Turbulent viscosity	(kg/(m·s))
U_{in}	Mean inlet velocity	(m/s)
Δp	Pressure drop	(Pa)

References

1. Qin T, Xu R, Jiang P, Wang H. Influence of straight tube on serpentine tube heat exchanger with supercritical pressure fluid. Appl Therm Eng. 2025;270:126212. [CrossRef].
2. Lin S, Zhou L. Enhanced cooling design of serpentine mini-channel for optimizing energy consumption in battery thermal management. Therm Sci Eng Prog. 2025;62:103625. [CrossRef].
3. Chen Z, Wang X, Bai B. Flow and heat transfer performance of supercritical CO_2 recuperator with serpentine channels at high thermal–hydraulic parameters. Appl Therm Eng. 2026;283:128886. [CrossRef].
4. Dong L, Xin Y, Wu X, Zhang R. Simulation study on enhanced heat transfer of annular inner rib tube in geothermal coaxial heat transfer wellbore. Case Stud Therm Eng. 2025;71:106177. [CrossRef].
5. Wei J, Chen N, Li L, Liu J, Zhao J, Wang C, et al. Effect of spoiler columns on heat transfer performance of aluminum nitride-based microchannel heat sink. Ceram Int. 2022;48(24):36226–37. [CrossRef].
6. Ahirwar BK, Kumar A. Effect of wire coil inserts on heat transfer enhancement and fluid flow characteristics of a double-pipe heat exchanger. J Therm Anal Calorim. 2024;149(7):3027–42. [CrossRef].
7. Singh SK, Kacker R, Gautam SS, Arora A, Shende V. Performance optimization of a single profile multi v-cut twisted tape insert in a double-pipe heat exchanger. J Therm Anal Calorim. 2025;150(19):15761–75. [CrossRef].
8. Marzouk SA, Almehmadi FA, Aljabr A, Kaood A. Performance analysis of twisted tape inserts and nanofluids in double-pipe helical coil heat exchangers. J Therm Anal Calorim. 2025;150(14):11197–211. [CrossRef].
9. Sahin M, Kilic M, Karadag MA. Investigation of heat transfer enhancement using hemispherical turbulators in a double-pipe regenerative heat exchanger with phase change material. J Therm Anal Calorim. 2025;150(13):10249–65. [CrossRef].
10. Shahsavar A, Eisapour M, Talebizadehsardari P. Experimental evaluation of novel photovoltaic/thermal systems using serpentine cooling tubes with different cross-sections of circular, triangular and rectangular. Energy. 2020;208:118409. [CrossRef].
11. Reddy DS, Khan MK, Awasthi K. Thermohydraulic performance of a novel curved serpentine coil. Phys Fluids. 2020;32(8):083609. [CrossRef].
12. Awasthi K, Reddy DS, Khan MK. Performance comparison among the variants of curved serpentine coil. Phys Fluids. 2021;33(7):073604. [CrossRef].
13. Sun S, Ma C, Wang X, Yang Y, Mei J. Design and optimisation of a novel serpentine flow channel with branch structure. Energy. 2024;293:130494. [CrossRef].
14. Singh P, Ji Y, Ekkad SV. Multi-pass serpentine cooling designs for negating Coriolis force effect on heat transfer: Smooth channels. J Turbomach. 2019;141(7):071001. [CrossRef].
15. Tanthadiloke S, Kittisupakorn P, Boriboonsri P, Mujtaba IM. Devise of a W serpentine shape tube heat exchanger in a hard chromium electroplating process. Chin J Chem Eng. 2019;27(1):218–25. [CrossRef].
16. Fathalla AS, Yassine HM, Nosier SA, Abdel-Aziz MH, Sedahmed GH, El-Naggar MA. Turbulent flow-driven liquid-solid mass transfer in serpentine tube heat exchanger/reactors: Applications and implications. Exp Heat Transf. 2024;37(7):1119–38. [CrossRef].
17. Zhang ZP, Wang K, Zhang X, Zhang ZD, Fan YH, Min CH, et al. Buoyancy influencing convective heat transfer characteristics of supercritical CO_2 in a serpentine solar receiver tube at low Reynolds number. Appl Therm Eng. 2024;240:122202. [CrossRef].
18. Han CL, Ren JJ, Dong WP, Bi MS. Numerical investigation of supercritical LNG convective heat transfer in a horizontal serpentine tube. Cryogenics. 2016;78:1–13. [CrossRef].
19. Wang Y, Ren JJ, Wang C, Bi MS. Mechanism analysis of the buoyancy effects on heat transfer of supercritical nitrogen in horizontal serpentine tube. Int J Heat Mass Transf. 2020;152:119417. [CrossRef].

20. Sun Y, Wang H, Nie F, Gong M, Shen J. Investigations on the heat transfer enhancement of converging minitubes for methane condensation. Int J Refrig. 2024;160:357–72. [CrossRef].
21. Xie X, Ye D, Wang J, Babaei M. A review on passive heat transfer enhancement techniques applied to supercritical thermal systems. Renew Sustain Energy Rev. 2026;235:116939. [CrossRef].
22. Choure BK, Alam T, Kumar R. A review on heat transfer enhancement techniques for PCM based thermal energy storage system. J Energy Storage. 2023;72:108161. [CrossRef].
23. Wang B, Lin J. Study on the dynamics and heat transfer characteristics of spherocylindrical particles in fluidized beds. Chem Eng Sci. 2026;325:123465. [CrossRef].
24. Kichatov B, Sudakov V, Korshunov A. Intensification of heat transfer using active bubble liquid. Phys Fluids. 2025;37(11):113304. [CrossRef].
25. Wang Q, Su L, Li C, Li X, Peng Z, Chen Q, et al. Improving heat transfer performance in serpentine microchannel with carbon nanotube-embedded PVDF coating. Case Stud Therm Eng. 2024;61:104946. [CrossRef].
26. Jia F, Zhang H, Zhang G, Wei M, Tian M. Study on the dynamics and heat transfer characteristics of droplet impact on hydrophilic-hydrophobic striped tube. Int J Heat Mass Transf. 2026;256:127983. [CrossRef].
27. Mebarek-Oudina F, Bouselsal M, Khan SU, Ramesh K, Ismail AI. Optimizing thermal performance in shell-and-tube heat exchangers with tri-hybridised nanofluids: A numerical study of turbulent convection. Therm Sci Eng Prog. 2025;65:103988. [CrossRef].
28. Fayz-Al-Asad M, Mebarek-Oudina F, Vaidya H, Hasan MS, Sarker MMA, Ismail AI. Finite element analysis for magneto-convection heat transfer performance in vertical wavy surface enclosure: Fin size impact. Front Heat Mass Transf. 2024;22(3):817–37. [CrossRef].
29. Kanti PK, Wanatasanappan VV, Said NM, Saini S, Mishra V, Paramasivam P, et al. Thermal performance, entropy generation, and machine learning insights of Al_2O_3-TiO_2 hybrid nanofluids in turbulent flow. Sci Rep. 2025;15:16035. [CrossRef].
30. Kanti PK, Vicki Wanatasanappan V, Mahjoub Said N, Sharma KV. Stability, thermophysical properties, forced convective heat transfer, entropy minimization and exergy performance of a novel hybrid nanofluid: Experimental study. J Mol Liq. 2024;410:125571. [CrossRef].
31. Liaw KL, Kurnia JC, Sasmito AP. Turbulent convective heat transfer in helical tube with twisted tape insert. Int J Heat Mass Transf. 2021;169:120918. [CrossRef].
32. Kurnia JC, Chaedir BA, Sasmito AP. Laminar convective heat transfer in helical tube with twisted tape insert. Int J Heat Mass Transf. 2020;150:119309. [CrossRef].
33. Bozzoli F, Cattani L, Mocerino A, Rainieri S, Pagliarini G. Experimental investigation on the convective heat transfer enhancement in tubes with twisted-tape inserts. J Phys Conf Ser. 2019;1224(1):012046. [CrossRef].
34. Chourasia S, Kumar A, Ahirwar BK. Numerical study of fluid flow and heat transfer in a circular tube with Trapezoidal-cut twisted tape inserts. J Therm Anal Calorim. 2024;149(17):9851–66. [CrossRef].
35. Marzouk SA, Aljabr A, Almehmadi FA, Sharaf MA. Enhancing heat transfer in a double-tube heat exchanger using perforated twisted tape and nanofluid. J Therm Anal Calorim. 2025;150(5):3719–33. [CrossRef].
36. Azmi WH, Sharma KV, Sarma PK, Mamat R, Anuar S. Comparison of convective heat transfer coefficient and friction factor of TiO_2 nanofluid flow in a tube with twisted tape inserts. Int J Therm Sci. 2014;81:84–93. [CrossRef].
37. Dhumal GS, Havaldar SN. Enhancing heat transfer performance in a double tube heat exchanger: Experimental study with twisted and helical tapes. Case Stud Therm Eng. 2023;51:103613. [CrossRef].
38. Eiamsa-Ard S, Nivesrangsan P, Chokphoemphun S, Promvonge P. Influence of combined non-uniform wire coil and twisted tape inserts on thermal performance characteristics. Int Commun Heat Mass Transf. 2010;37(7):850–6. [CrossRef].
39. Heeraman J, Kumar R, Chaurasiya PK, Ivanov Beloev H, Krastev Iliev I. Experimental evaluation and thermal performance analysis of a twisted tape with dimple configuration in a heat exchanger. Case Stud Therm Eng. 2023;46:103003. [CrossRef].
40. Kumar A, Ali MA, Maithani R, Kumar Gupta N, Sharma S, Kumar S, et al. Experimental analysis of heat exchanger using perforated conical rings, twisted tape inserts and CuO/H_2O nanofluids. Case Stud Therm Eng. 2023;49:103255. [CrossRef].